TIARA-NOTE-WP9-2014-002


Test Infrastructure and Accelerator Research Area

**Scientific / Technical Note**

# Thermal-hydraulic analysis of the neutron source for T-MIF

Fusco, Y. (CERN) *et al*

12 February 2014

The research leading to these results has received funding from the European Commission under the FP7-INFRASTRUCTURES-2010-1/INFRA-2010-2.2.11 project TIARA (CNI-PP). Grant agreement no 261905.

This work is part of TIARA Work Package **9: TIHPAC R&D Infrastructure**.

The electronic version of this TIARA Publication is available via the *TIARA web site* at `http://www.eu-tiara.eu/database` or on the *CERN Document Server* at the following URL: `http://cds.cern.ch/search?p=TIARA-NOTE-WP9-2014-002`


Test Infrastructure and Accelerator Research Area

# Technical Note

# Thermal-hydraulic analysis of the neutron source for T-MIF

**Fusco Y.; Behzad M. (CERN)**

**3. February 2014**

The research leading to these results has received funding from the European Commission under the FP7-INFRASTRUCTURES-2010-1/INFRA-2010-2.2.11 project TIARA (CNI-PP).
Grant agreement no 261905.

This work is part of TIARA Work Package 9: TIHPAC R&D Infrastructure.



# TIARA Project

## Work Package 9: TIHPAC - Test Infrastructure for High Power Accelerator Components

## Task 9.1: Multi MW Irradiation Facility for complex target testing

## TN n ° 02: Thermal-hydraulic analysis of the neutron source for T-MIF

**Planned Date (month):36**

**Achieved Date (month):38** **(contribution to final report due month 36)**

**Lead Contractor:CERN**

---

| | |
|---|---|
| **Project acronym:** | *TIARA* |
| **Project full title:** | *Test Infrastructure in Accelerator Research Area* |
| **Start of the Project:** | *1st January 2011* |
| **Duration of the project:** | *36 Months* |
| **Authors:** | *Yoann Fusco*<br>*Design engineer*<br>*Masoud Behzad*<br>*PhD Student* |
| **Lead engineer:** | *Karel Samec*<br>*Nucl. Eng., Mech. Eng.* |
| **Task Coordinator:** | *Yacine Kadi*<br>*Prof. Dr. Phys.* |

# *C o n t e n t s*

## *F i g u r e s*

## *T a b l e s*

## *R e f e r e n c e s*

*Ref. 1: K. Samec: "Report on the Definition and Specifications of the Irradiation test Facilities", TIARA deliverable MS33, FP7-Infrastructures-2010-1/INFRA-2010-2.2.11 project TIARA, 23 January 2012*

*Ref. 2: K. Samec: "Preliminary design report for a high-power Material Irradiation Facility T-MIF", TIARA Deliverable MS34, FP7-Infrastructures-2010-1/INFRA-2010-2.2.11 project TIARA, 25 February 2013*

*Ref. 3: R. Luis, Y. Romanets : "Neutronics FLUKA analysis of the Target section for T-MIF", TIARA-REP-WP9-2014-XXX, FP7-Infrastructures-2010-1/INFRA-2010-2.2.11 project TIARA, January 2014*

*Ref. 4: Y. Fusco "Detail Engineering Design T-MIF", TIARA-REP-WP9-2014-XXX, FP7-Infrastructures-2010-1/INFRA-2010-2.2.11 project TIARA, January 2014*

## *S y m b o l s*

Parameters, variables and abbreviations:

| | | |
|---|---|---|
| CERN | Abbr. | Centre Européen de la Recherche Nucléaire, Switzerland |
| $C_P$ | [J/kg/K] | Thermal capacity |
| CFD | Abbr. | Computational Fluid Dynamics |
| dpa | Abbr. | Displacement per atom |
| FEM | Abbr. | Finite Element Method |
| $f$ | [Hz] | Frequency |
| LM | Abbr. | Liquid Metal |
| T | [°C] | Temperature |
| t | [sec.] | Time |
| $\Delta$ | [-] | Discrete difference, change |
| $\phi$ | [n/cm$^3$/s] | Neutron flux |
| $\lambda$ | [W/m/s] | Thermal conductivity |
| $\rho$ | [kg/m$^3$] | Density |

# 1 Design of the T-MIF neutron source

The preliminary design report (Ref. 2) laid out in principle the design of the T-MIF neutron source inspired by prior experience in the EURISOL program. The possibility of irradiating samples under combined proton and neutron irradiation was investigated in the specification report (ref.2), which suggested using an elliptical beam impacting the sample side-on. In so doing, it was hoped a fairly homogeneous DPA distribution would be reached in the sample, a fact borne out by later neutronic analysis (ref.3)

The sample disposition and the necessity to house the loading mechanism meant the target had to be widened in the plane of the sample (ref.2 & 4). Furthermore the elliptical section of the beam meant the original circular symmetry of the EURISOL target was deemed to be not optimal for minimising thermal stresses. Hence the EURISOL target beam window was changed from a circular symmetry to an elliptical cross-section in a plane at right angle to the beam. Along the beam direction however, the beam window section was kept the same as in the original neutron source.

These changes in the beam window, entail the local speed distribution along its wetted surface may be altered, thereby modifying the cooling characteristics and *in fine* the beam window temperature.

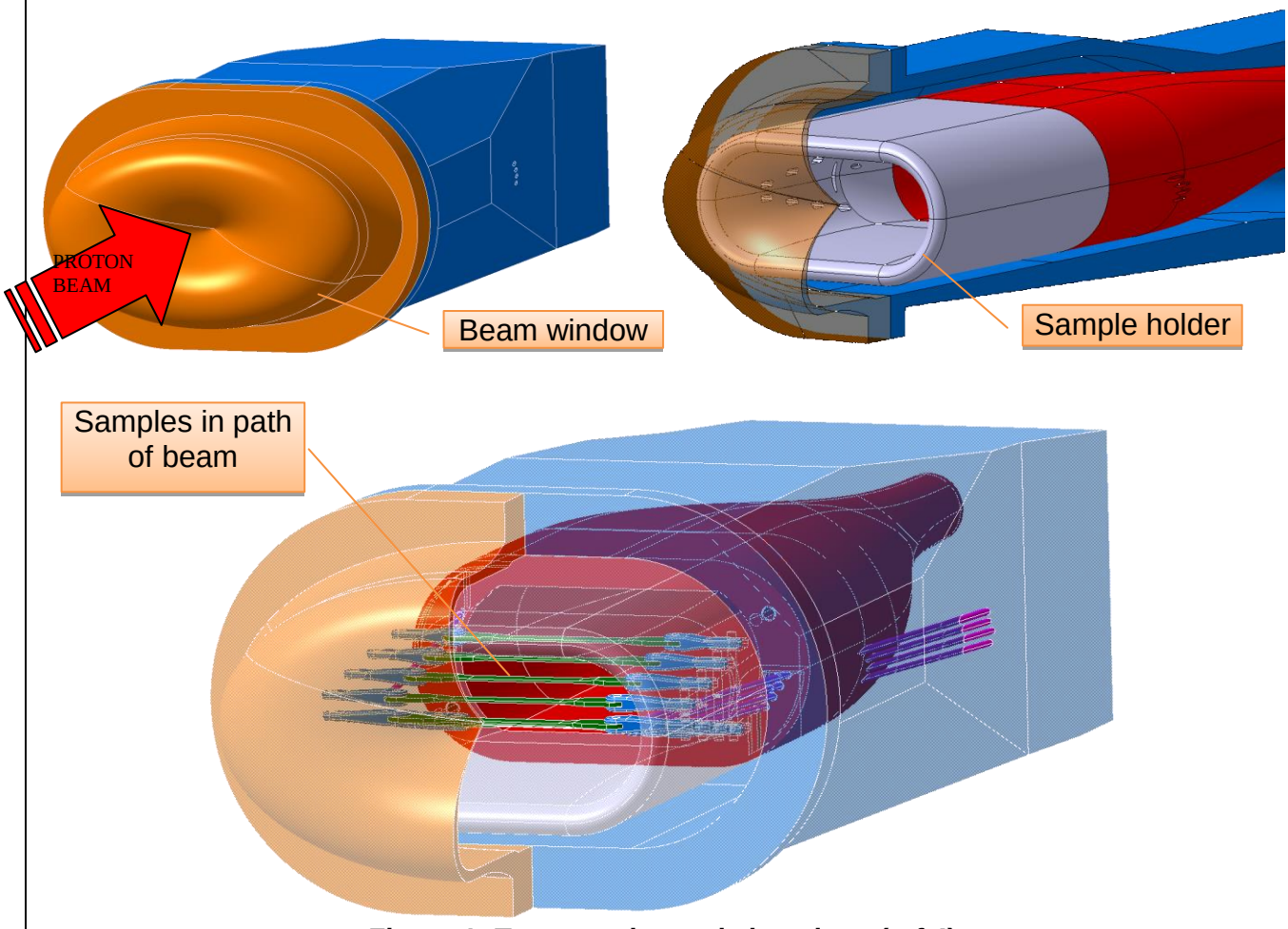


**Figure 1: Target and sample locations (ref.4)**

# 2 Fluid dynamic optimisation of the neutron source

## 2.1 Assumptions and Boundary conditions

The initial simulation focuses only on the hydraulics, i.e. ensuring stable flow exists over the window. To this end, it is not necessary to include the effect of the beam as the temperature increase in the liquid metal will be low enough to ensure that buoyancy effects are modest in relation to the overall speed of the liquid metal. Hence wherever the purpose of the analysis is to optimise the flow, heat deposition is not considered, as the additional equations which need to be computed, slow down numerical convergence.

Heat deposition is considered when the temperatures in the window, sample and fluid are needed. Therefore, in order to further simplify the calculation, in some calculations where the heat deposition is not considered, the entire sample loading mechanism is removed from the CFD model as is the structure itself. The model then only contains the fluid domain bounded by what are essentially adiabatic walls. This is an appropriate simplification since the main objective of such optimisations is to verify the flow on the beam window and the mechanism is located downstream of the window.

Based upon the heat exchanger calculations documented in Ref.4, the following boundary conditions are applied in the CFD simulations hereafter:

Inlet mass flow rate is set at 4,1 kg/s

Inlet temperature is 380 °C.

Outlet: the static pressure is 0 bar

The nominal pressure of the fluid is 1 bar.

The turbulence model used is the SST

## 2.2 Design iterations to optimise the flow in the target

The design must be able to function over a wide range of speeds so as to allow the temperature in the sample to be varied. The source of heat, the beam is constant as is the deposition in the sample. The simplest method of controlling the sample temperature is therefore to change the flow rate, another method would be to apply electric heating to the sample but this could be a challenge in an electrically conductive medium.

At first the design proposed in ref.2 is examined at a speed sufficient to keep the samples at temperatures close to the DBTT of austenitic stainless steel under high irradiation dose. The nominal flow rate is multiplied by roughly a factor of 10. This will raise pressure losses in all components, most notably the target which is therefore the main focus of the CFD analysis. The heat exchanger can be expected to perform better at the higher flow rate and is therefore not examined in the current context.

### 2.2.1 Iteration 0

The analysis for this initial examination was conducted at maximum speed on the original design shown in Ref.2. The maximum speed corresponds to a flow rate of 38 kg/s not 4.1 kg/s which is the baseline. In doing so, the temperature in the sample can be lowered to 400°C (refer to chapter 3). The rationale for varying the speed is to vary the temperature in the sample and since the highest speed presents the greatest challenge in terms of stability, the initial iteration focused on this domain. Furthermore, the heat exchanger can be expected to function far better at higher speeds and it is therefore only necessary to focus on the target, not on the rest of the system.

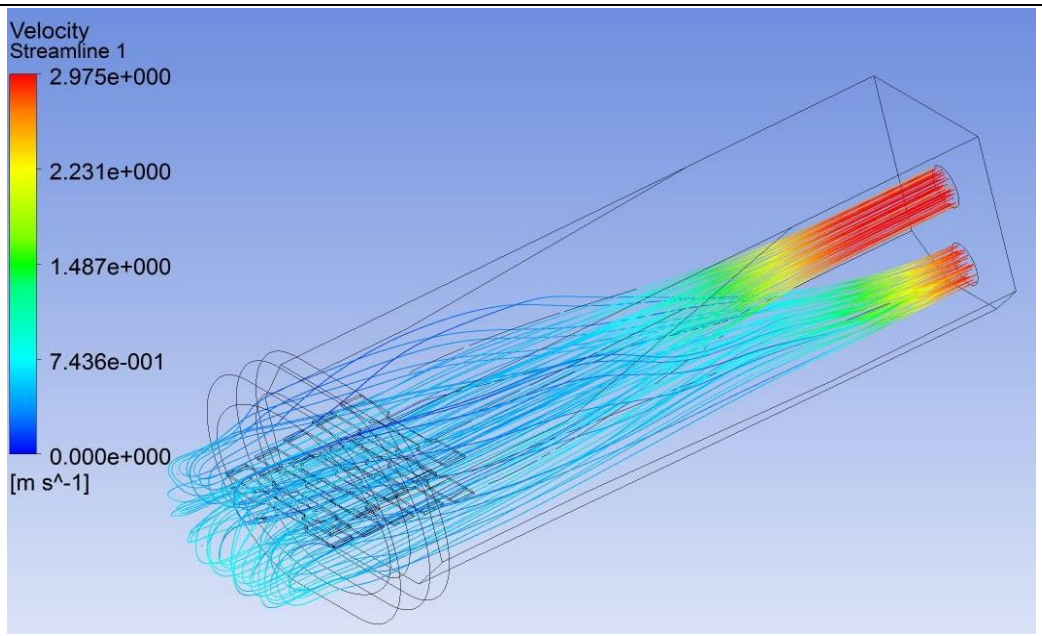


**Figure 2: Velocity streamlines in the fluid**

The initial calculation shows some interesting features in the flow pattern. Although this may not immediately visible in the figure above, closer examination of the flow field in the annular section just upstream of the window shows there is an imbalance between the lower an upper section. More fluid is conducted through the lower portion of the annulus which could result in an unsteady flow further downstream. Hence in order to ascertain the level of imbalance measurements thereof are taken along the beam axis in the model using sections perpendicular to the beam axis, shown in red in the figure below.

An attempt was made to find how to equalize this flow and it was suggested that lengthening the target would give the incoming flow in the annulus the space needed to equalize between the top and bottom of the channel. In order to quantify this proposition, the flow at different sections was examined as shown in the figure below,

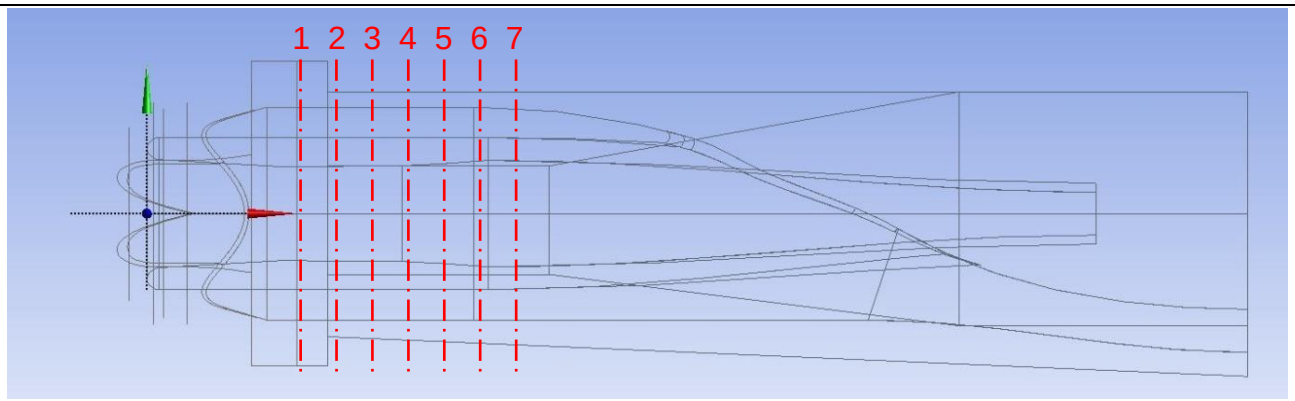


**Figure 3: Side view showing section planes for calculating the flow imbalance**

The velocity contours in the sections planes are shown in the next following figure, illustrating how the imbalance becomes progressively weaker along the incomer annulus, just before reaching the window. However the imbalance does not completely disappear, and is the focus of a detailed calculation.

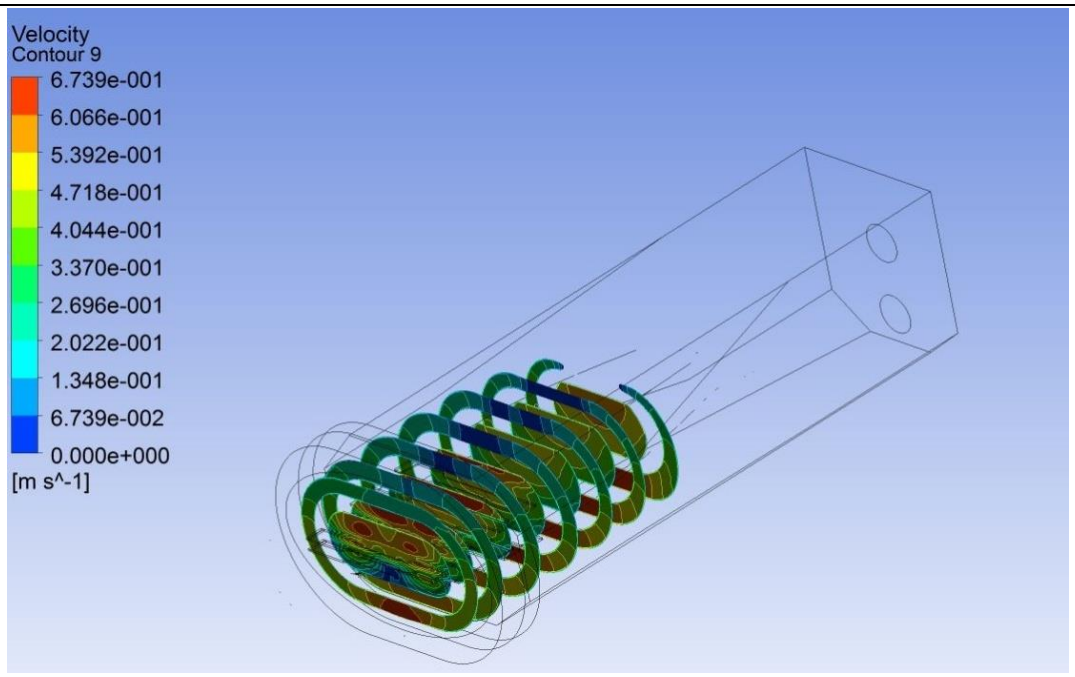


**Figure 4: Velocity contour in the annulus and guide tube**

In order to find the imbalance between the integrated flow in upper and lower regions of the incomer annulus, the average velocity is computed in each section plane, for the top and bottom as given in Table 1. Note that after plane 4, the ratio does not change.

To find the required additional length of the target, the "x" corresponding to an imbalance equal to 1 must be found, as this corresponds to a flow in the incomer annulus where there is no difference between the upper and lower flow. There are two possibilities top interpolate the results; an exponential or a linear interpolation. According to an exponential interpolation, the imbalance=1 is reached at coordinate 3.5cm. Based on a linear interpolation, imbalance is resolved at 4.5[cm]. This corresponds to a needed increase in length of 6[cm]. Conservatively, the target is lengthened by 10[cm].

| | Y(cm) | Imbalance |
|---|---|---|
| Plane 1 | 7 | 2.19 |
| Plane 2 | 10 | 2.83 |
| Plane 3 | 15 | 5.50 |
| Plane 4 | 20 | 19.0 |
| Plane 5 | 25 | 18.8 |
| Plane 6 | 30 | 19.0 |
| Plane 7 | 35 | 19.0 |

**Table 1: Flow Imbalance in each plane**

The target is thus to be lengthened by an additional 10 cm to allow the flow more running length for equalising its distribution over the entire section of the annulus before the beam window. This should be sufficient to guarantee stable conditions on the window. Furthermore, on the whole, there seems to be adequate cooling of all the structural parts particularly the samples which are at fairly constant

temperature. Therefore subsequent iterations will focus on enhancing the stability of the flow on the window with the target increased by the required 10cm.

### 2.2.2 Iteration 1

In this design configuration the fluid is entering into the target station from the side in order to allow greater depth for the shielding. Indeed, a greater thickness of polyethylene has to be added behind the target as compared to the sides of the target because the more energetic particles escape from the target rear section (see ref.3). Hence having straight pipes at the back would act as an escape route for gammas and neutrons leaking form the target.

Since the overall dimensions of the T-MIF facility are to be reduced as much as possible, bending the pipe just after the active section of the target may be thought to bring some advantage.

However the flow in the CFD simulation appear to show that this configuration makes the fluid turn on itself precisely in the regions where the samples are to be located and in addition creates a vortex in the window. Although the second aspect could in theory bring about a higher velocity on the window and thus better cooling it is also much more unstable. The vortex around the samples is far more problematic, it could lead to a high amount of turbulent detached flow on the samples which would then no longer be kept at constant temperature, a mandatory requirement for providing adequate data for material research purposes.

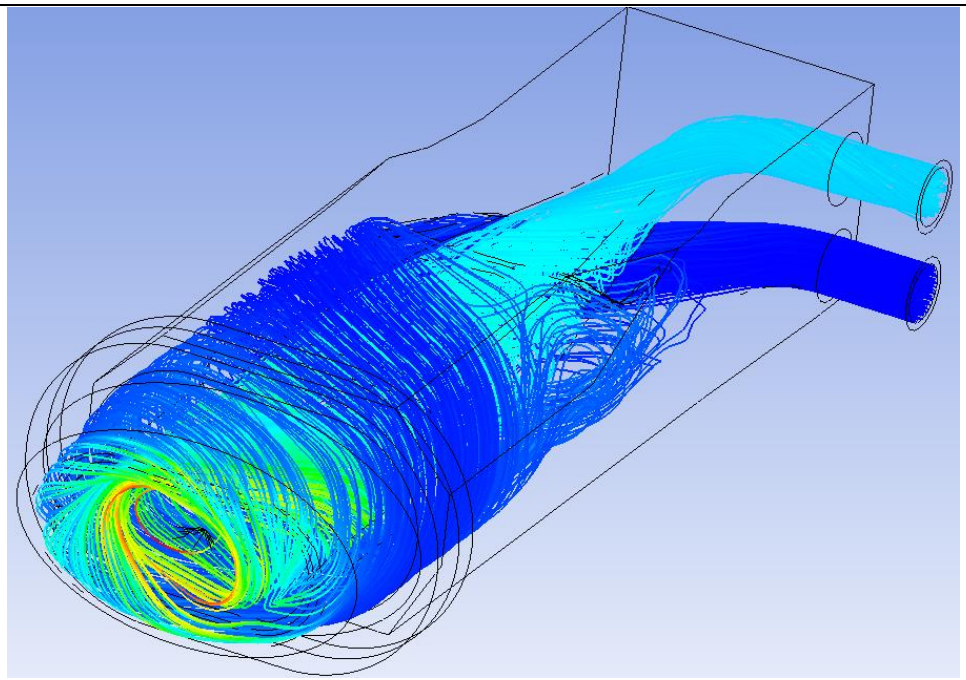

**Figure 5: Velocity streamline with an interface facing sideways**

The conclusion from the previous calculation is that in- and outlet pipes have to be straight behind the target station to avoid this phenomenon. Furthermore, new results from the neutronic calculation show that a lead shielding would be more efficient than polyethylene behind the target as the liquid lead in the target itself would also be of benefit as a shielding against gammas, post shutdown.

### 2.2.3 Iteration 2

In the current iteration, the interface has been moved back to the rear of the target. A totally new flow field appears which although more steady is still highly complex.

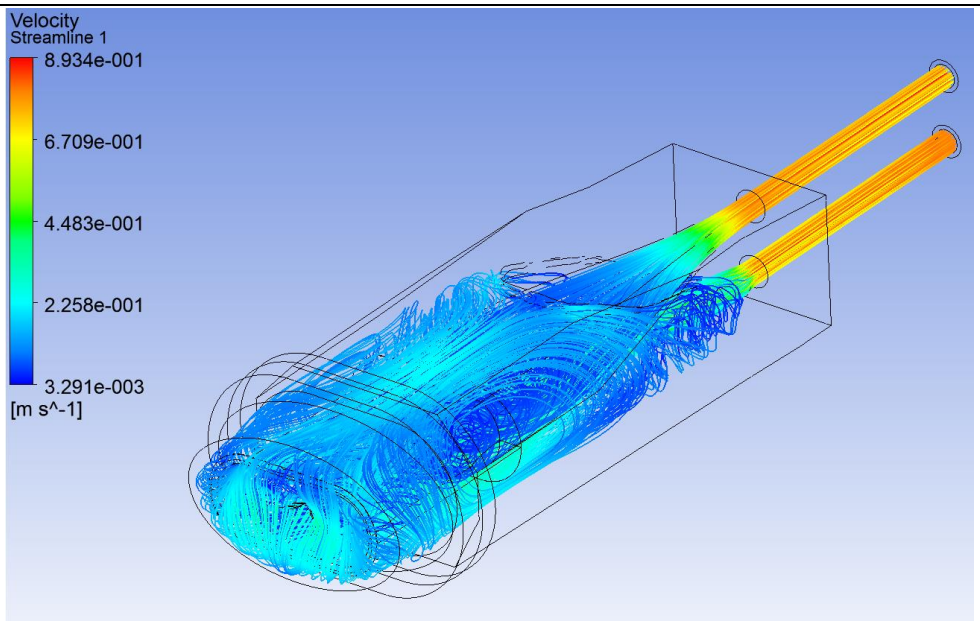


**Figure 6: Velocity streamline with rear interface**

Flow problems in the fluid point to additional areas needing improvement. First the inlet is too wide and forces the fluid to recirculate inside the incomer annulus tube instead of flowing steadily towards the window. The space between the exit collector and the chassis is too great compared to the incomer annulus such that the fluid cannot fill this space entirely and stays in the lower portion of the chassis instead of flowing back out the exit collector. Finally, the space between the window and the front of the sample holder is also too wide, so that the fluid flows over the sample holder but loops back towards the window instead of being guided into the sample holder. All these matters have to be resolved and the design needs to be improved in order to guide the fluid flow better.

### 2.2.4 Iteration 3

In this iteration, the annulus section is slightly raised and its axis follows an arching curve at the entrance to attempt to force the fluid to move upwards, around the exit collector and the sample holder. The illustration below shows that the fluid is accelerated along the lower section and most of the problems described above remain.

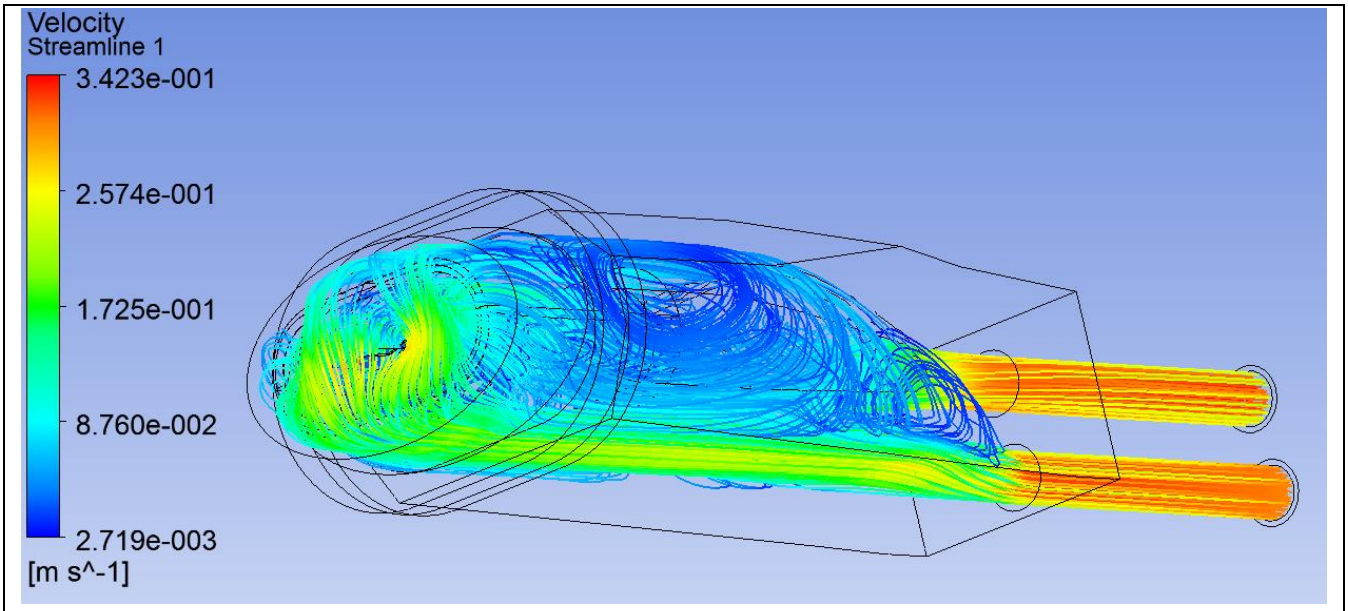


**Figure 7: Incomer annulus shifted vertically upwards**

### 2.2.5 Iteration 3

After a number of intermediate iterations which are not documented here, the incomer annulus is shifted to a position in vertical direction which seems to result in acceptable flow pattern. There is no direct recirculation and the fluid is directly fed more equally into the target. But the space after the window is still not filled entirely and the flow back from the window does not guide enough liquid equally all through the sample holder.

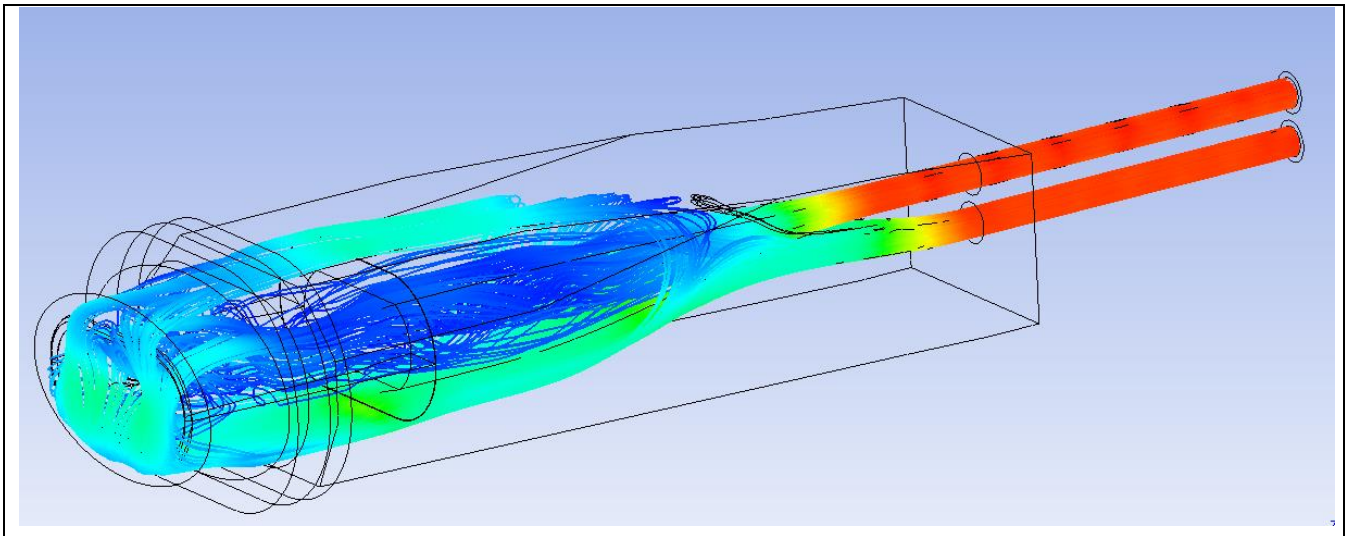

**Figure 8: Optimised incomer annulus position**

### 2.2.6 Iteration 4

Further modifications are implemented in the incomer annulus section, which is significantly reduced. Also the overall shape of the leading edge of the sample holder is modified to conform better to the elliptical section of the window. The fluid fills the whole volume of this modified incoming annulus and conforms to the window cusp as required in order to enter the sample holder smoothly.

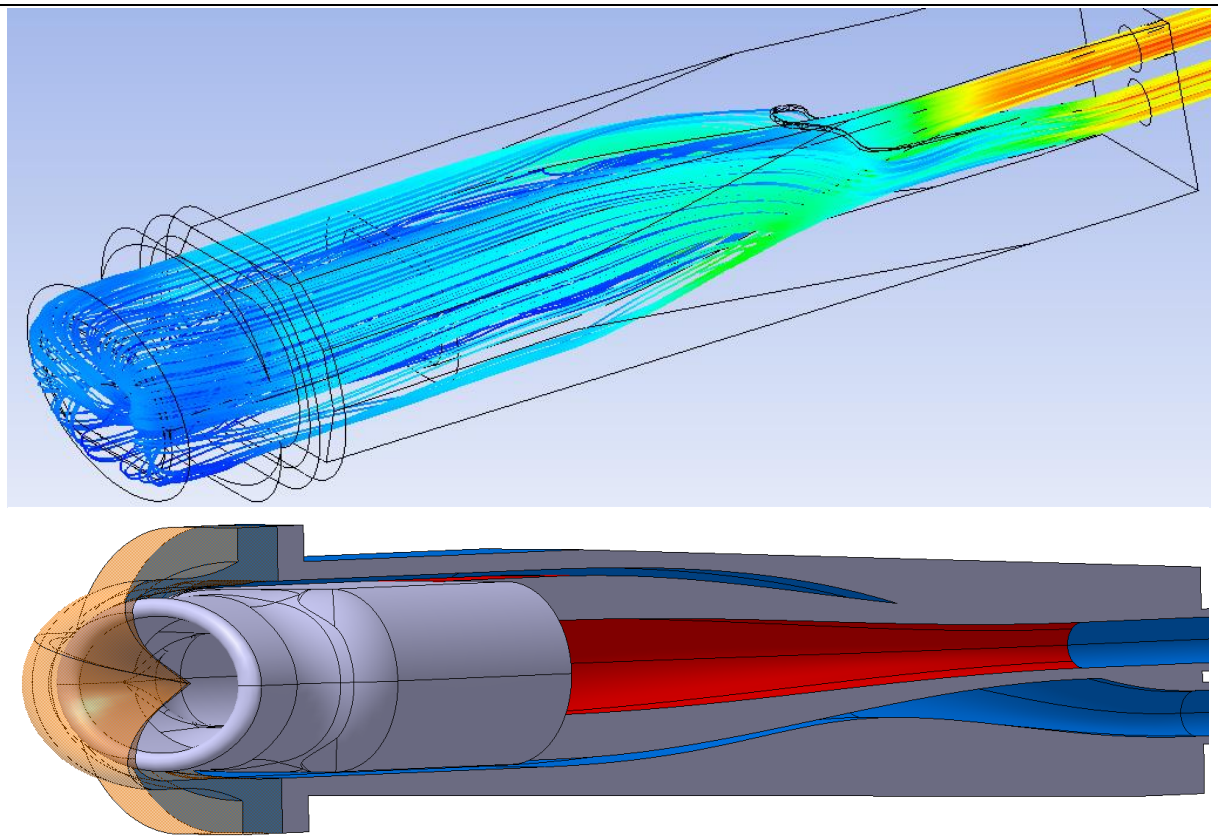

**Figure 9: Optimised incomer annulus thickness (top) and redesigned section (bottom)**

Having completed an optimisation on the inflow in the incomer annulus, some work is still needed on the outflow, beginning in the sample holder just after the window. Indeed, the following image shows a recirculation at the entrance of the sample holder, where the heat deposition is the highest.

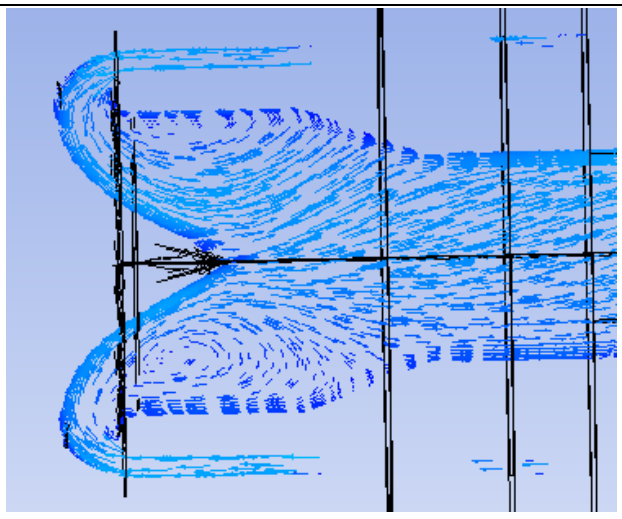

Figure 10: Recirculation in the sample holder

### 2.2.7 Iteration 5

The entrance surface of the sample holder is modified to avoid recirculation in the sample holder as shown above in the previous iteration. The new shape allows the flow to be guided back towards the exit more smoothly.

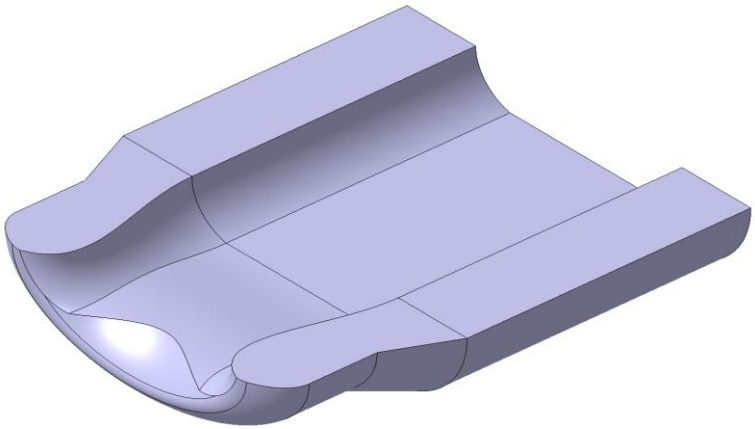

**Figure 11: Redesign of the sample holder**

This modification has a clear benefit in the vertical section but a significant recirculation is still observable in the horizontal section. As it occurs precisely in the region of the beam deposition, it would accumulate significant heat in the structure of the guide tube. Note however that in the absence of the samples, the recirculation is unhindered. This is a conservative model as the samples would effectively at the very least inhibit or perhaps even prevent such a recirculation from occurring.

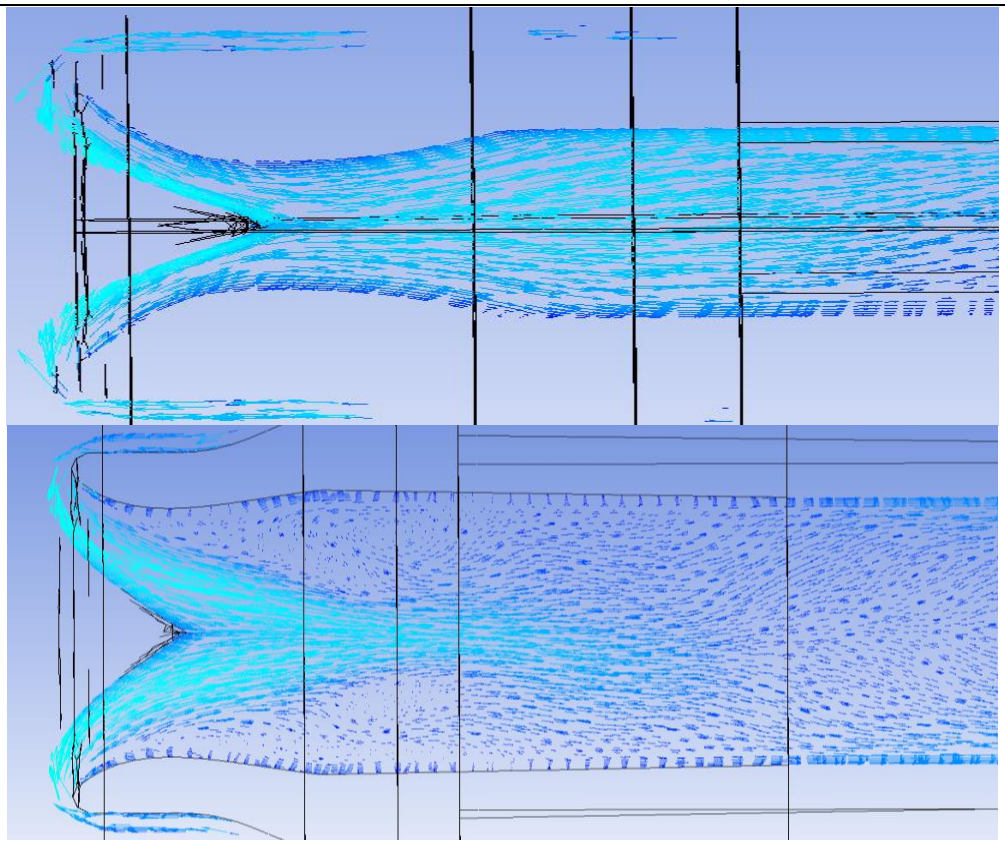

**Figure 12: Flow in the optimised sample holder vertical (top) and horizontal (bottom) Plane**

### 2.2.8 Iteration 6

In the next iteration, guide vanes are included to interfere with the recirculation pattern shown in the previous iteration. They succeed in isolating the high deposition region from the recirculation pattern, which thereby shifts towards the wall of the guide tube. Although this is not yet totally satisfactory, it yields a significant improvement. In the first example (left bottom in Figure 13), the position of the blade is not an optimum and does not maximise its impact on the flow distribution. New iterations are then undertaken (right bottom in Figure 13), to find the blade position which can generate a more stable flow.

From a structural point of view, these guide vanes are solidly anchored to the guide tube (see lower portion of figure below). They are an integral machined feature of the guide tube. It is therefore unlikely that they would rupture due to fatigue.

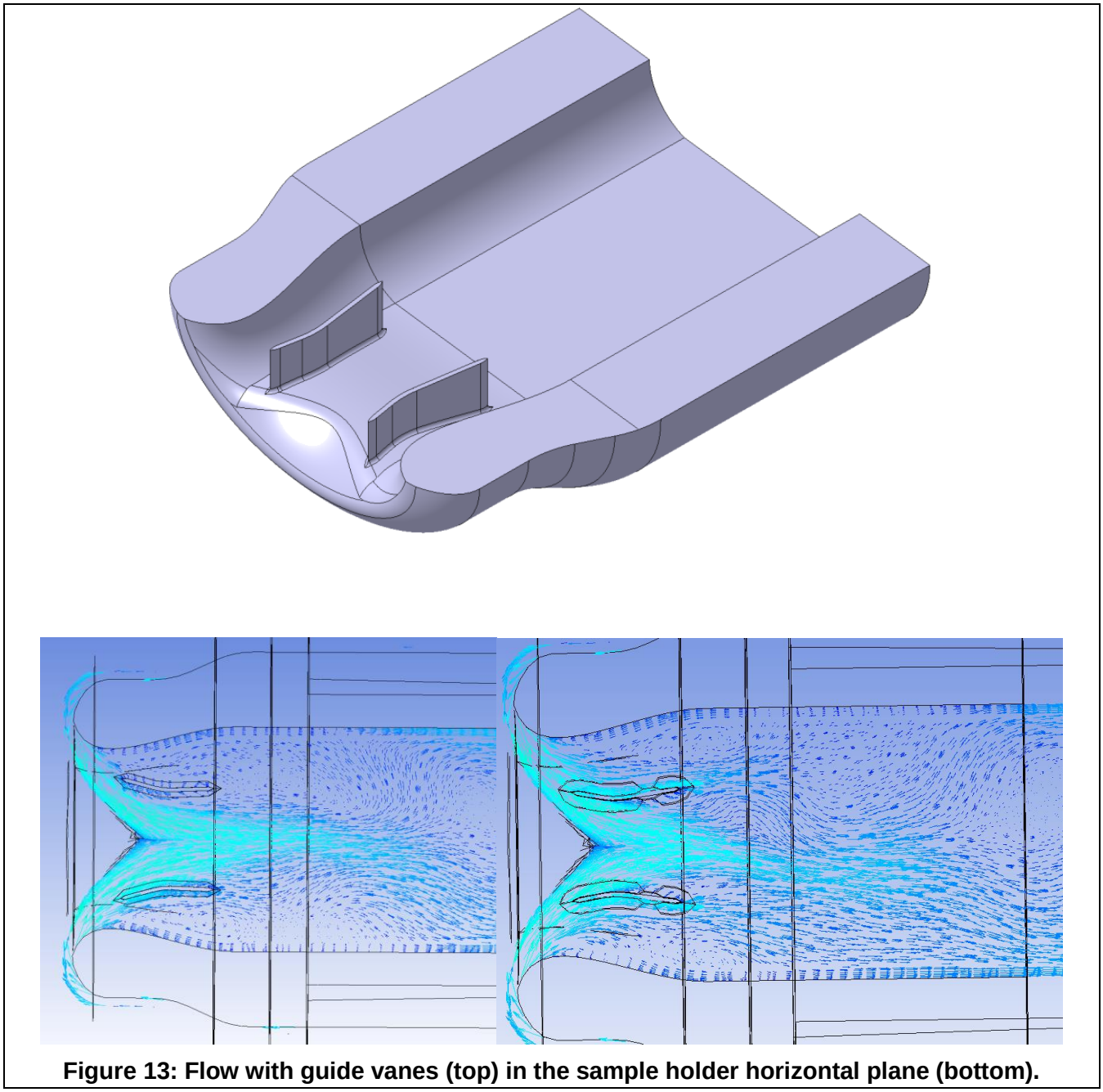

**Figure 13: Flow with guide vanes (top) in the sample holder horizontal plane (bottom).**

### 2.2.9 Iteration 7

Building on the previous attempt the guide vanes are doubled, which seems to have a favorable effect on the flow. Indeed the flow in the center of the exit channel in the sample holder is now widened.

Again, a few iterations were necessary to derive the most efficient position as may be seen in the next following figure.

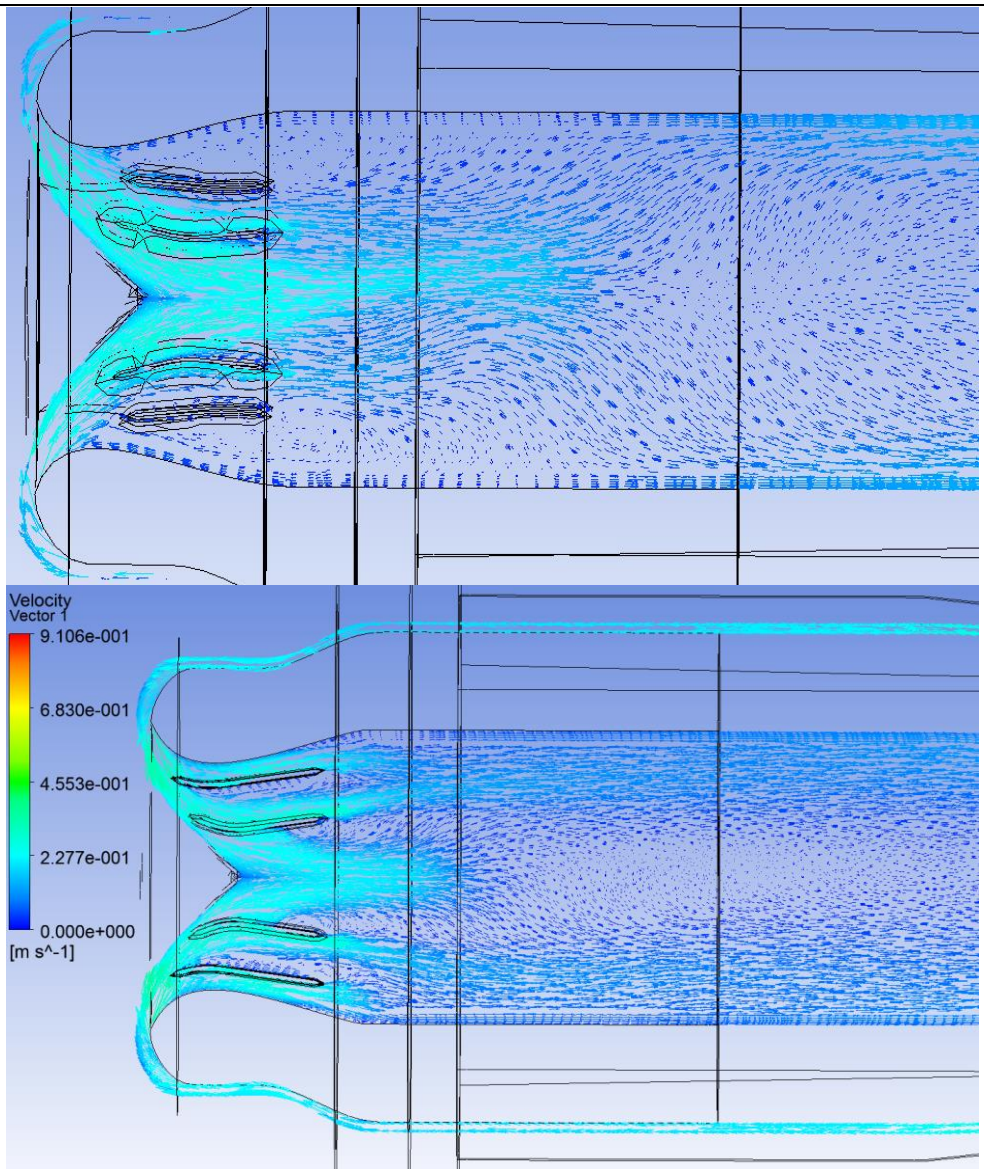


**Figure 14: Flow in the sample holder horizontal plane with two guide vanes at different positions**

It is now possible with the last iteration to suppress recirculation in the sample holder to avoid any overheating of the guide tube.

The resulting design is shown in the figure hereafter.

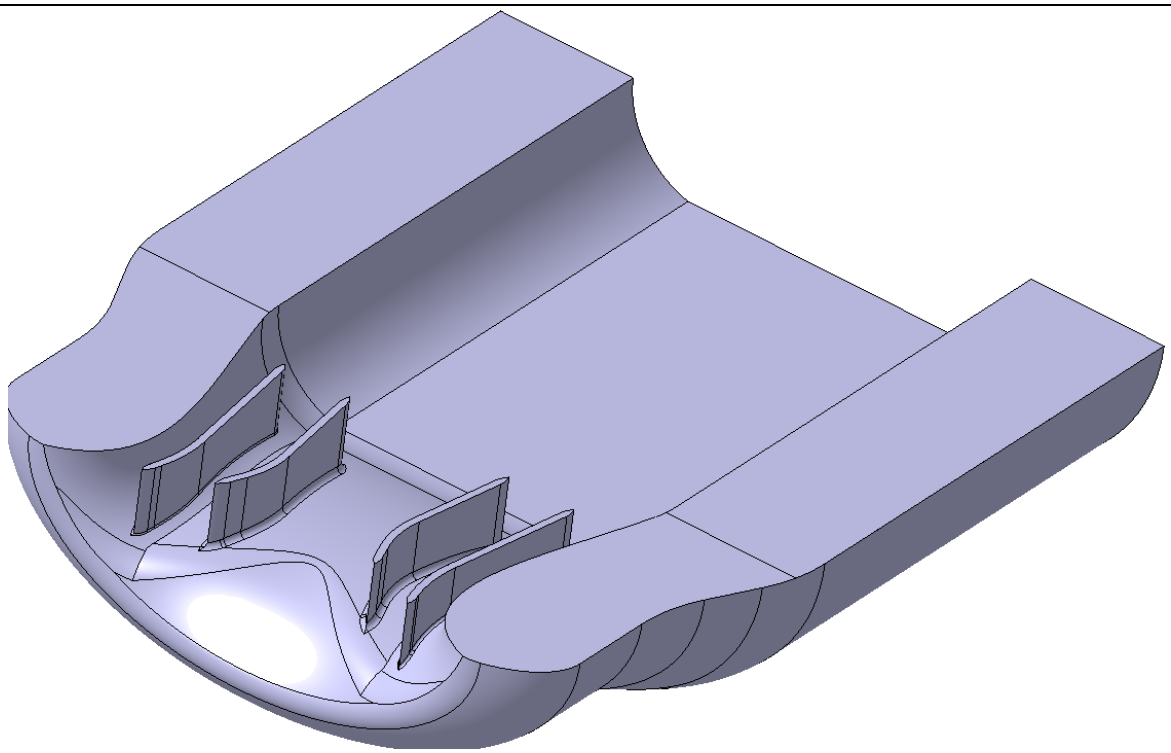

**Figure 15: Sample holder design with two guide vanes**

In light of the differences in hydraulic section between the window and the sample holder, the velocity decreases down to 0,1 m/s in the sample holder whereas it reaches 0.5 m/s at the inlet. The pressure into the fluid increases slightly during its passage in the target where it is fairly constant. Because of the low velocity the pressure drop is not significant although this may be an underestimation due the absence of the samples.

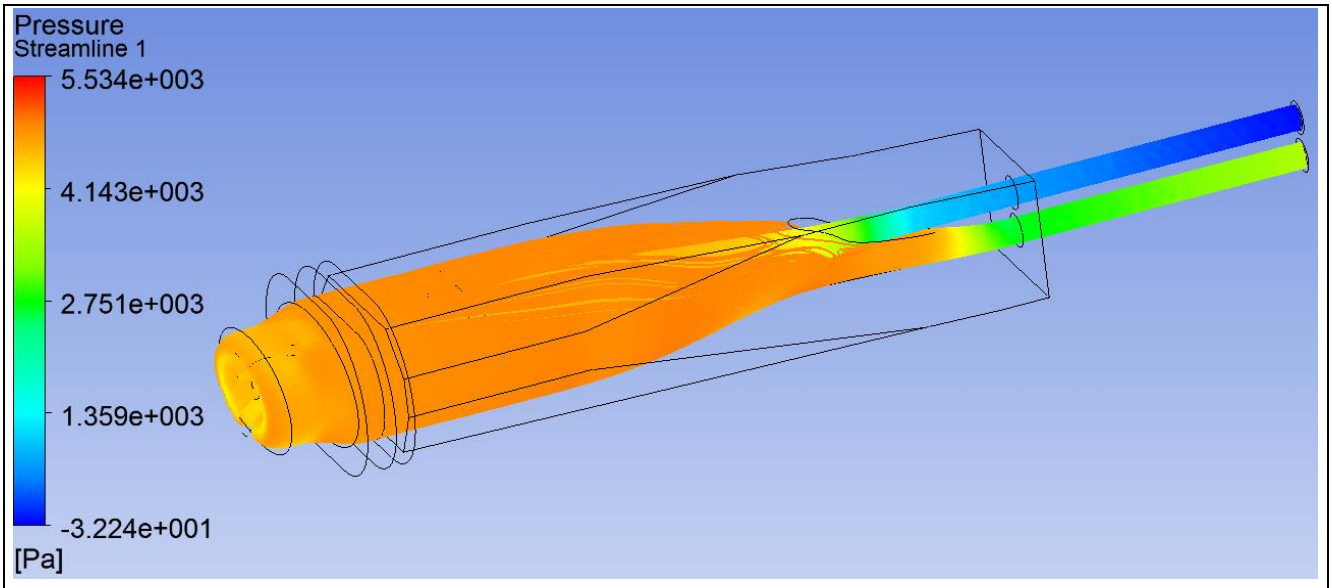


**Figure 16: Pressure drop along streamlines in final configuration**

Thus the final design of the target is derived, for which the sample mechanism will have to be adapted. This is however not anticipated to present any significant difficulty and will be integrated in a follow-on activity after the current design study.

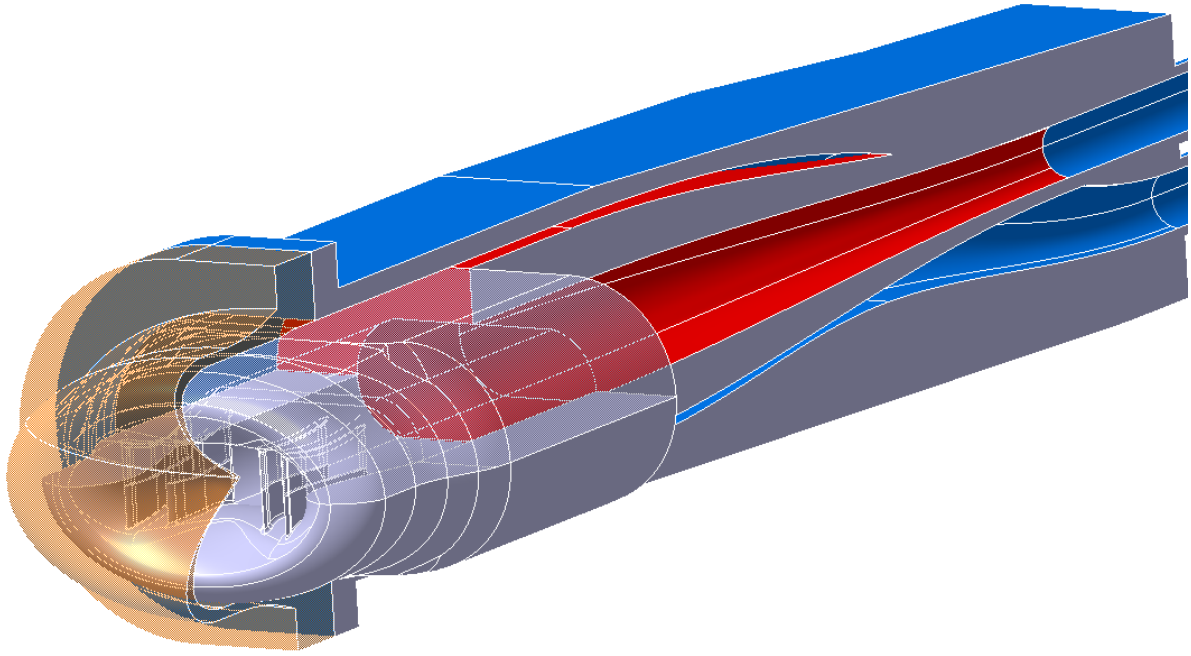

**Figure 17: Final optimised target configuration**

# 3 Thermal assessment of the design

## 3.1 Analysis of the initial design

The design proposed in ref. 2 is analysed in the current section. The subsequent iterations which were the focus of the previous chapter were not available at the time of this first calculation which was intended as a scoping analysis to test the thermal-hydraulic performance at maximum speed. Results for lower speeds will be derived in the next section.

The current analysis is therefore conducted using boundary conditions, which were modified compared to those outlined in the previous chapter. In this section a maximum of 38 kg/s was applied instead of the 4.1 kg/s stipulated in the chapter above.

Transient analysis is used in order to help in the convergence as the flow with the heat deposition from the beam is quite complex, hence the fluid flow is analysed over a total time of 10 seconds with 0.005 time increments, ramping up the applied boundary conditions linearly as illustrated in the figure below. As the heat of the beam deposition is considered, the thermal energy model is applied for heat transfer analysis in the fluid domain.

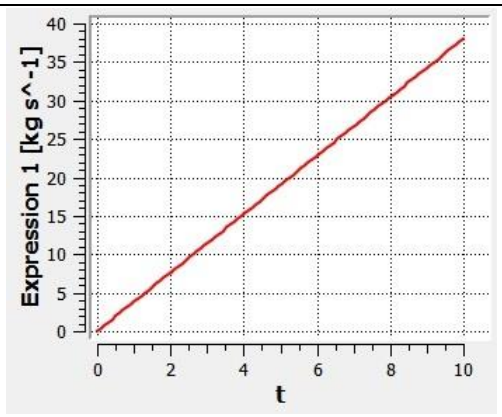


**Figure 18: Time dependent mass flow rate for inlet in fluid domain**

In this analysis the energy deposition is a parameter which must be considered. There are three main regions in which heat is deposited, the window, the samples and the fluid. Two expressions have been defined in CFX setup:

**Energy Deposition in the Fluid**

A*8.103*1.0e8[W/m^3]*exp{-(y-.03125[m])/0.15[m]}*{1-exp[( (y.03125[m])+0.045[m])/0.04[m] ] }*
{1+460[m^-1]*[0.267[m]-(y-0.03125[m])]*exp[-abs(0.267[m]-(y-0.03125[m]))/0.005[m] ] }*
exp{-0.5*[(z/0.012[m])^2+(x/0.0435[m])^2] }*cutoff*time

in which

A= 0.167*1.7;

time= (2/(pi[rad]))*atan(20 [s^-1]*t)

cutoff= step((y-0.03125[m])*1[m^-1])

**Energy Deposition in the Window**

A*4.8565*1.0e8[W/m^3]*exp(-0.5*((z/0.0115[m])^2+(x/0.069[m])^2))*time

**Energy Deposition in the samples**

Conservatively, the same deposition is used in the samples as in the fluid. In reality due to the lower density of most samples as compared to the fluid (Lead), the samples should be subjected to a lower heat deposition from the beam.

In the model, a patch-conforming method of meshing has been used in both solid and fluid parts; an inflation method is applied in the fluid region near the wall to capture the boundary layer.

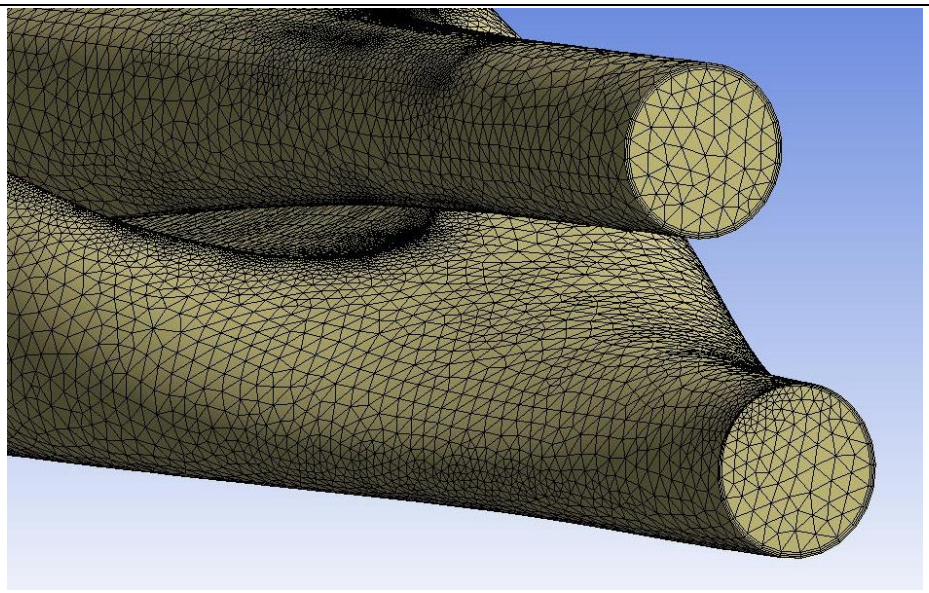

**Figure 19: Mesh in the fluid domain**

In a first calculation using the initial design, all assumptions here above including the heat deposition, are considered so as to verify whether the temperature lie in the desired envelope and whether system level parameters such as the pressure loss is acceptable. The results of this first calculation on the initial design re shown in the next following figures.

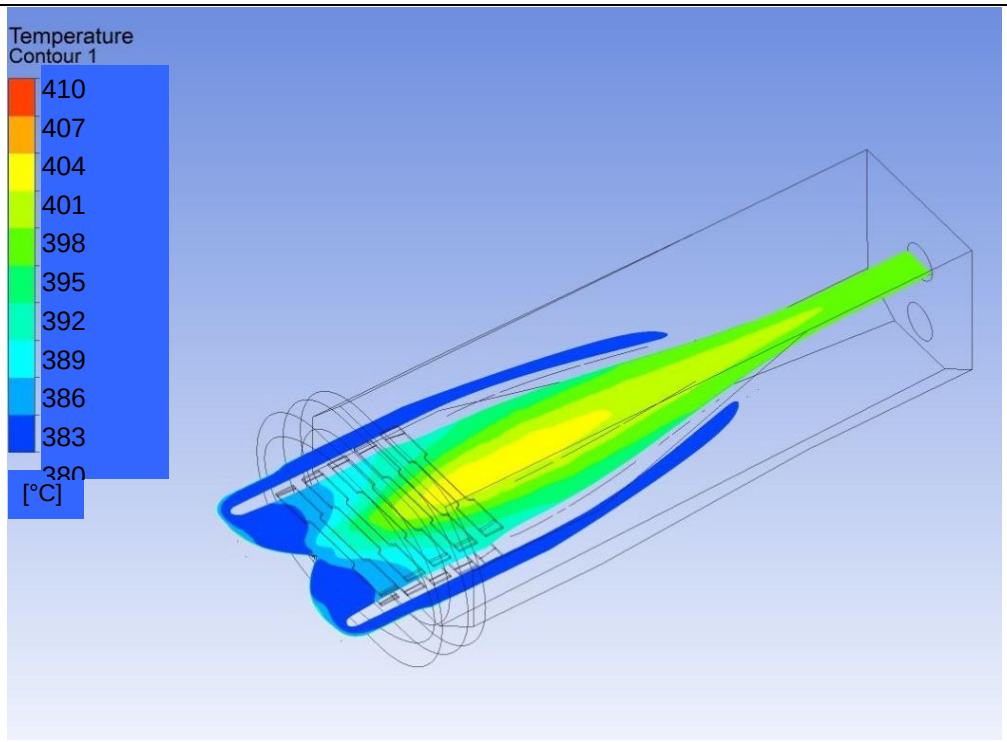


**Figure 20: Temperature contour in central plane in fluid region at 38 kg/s**

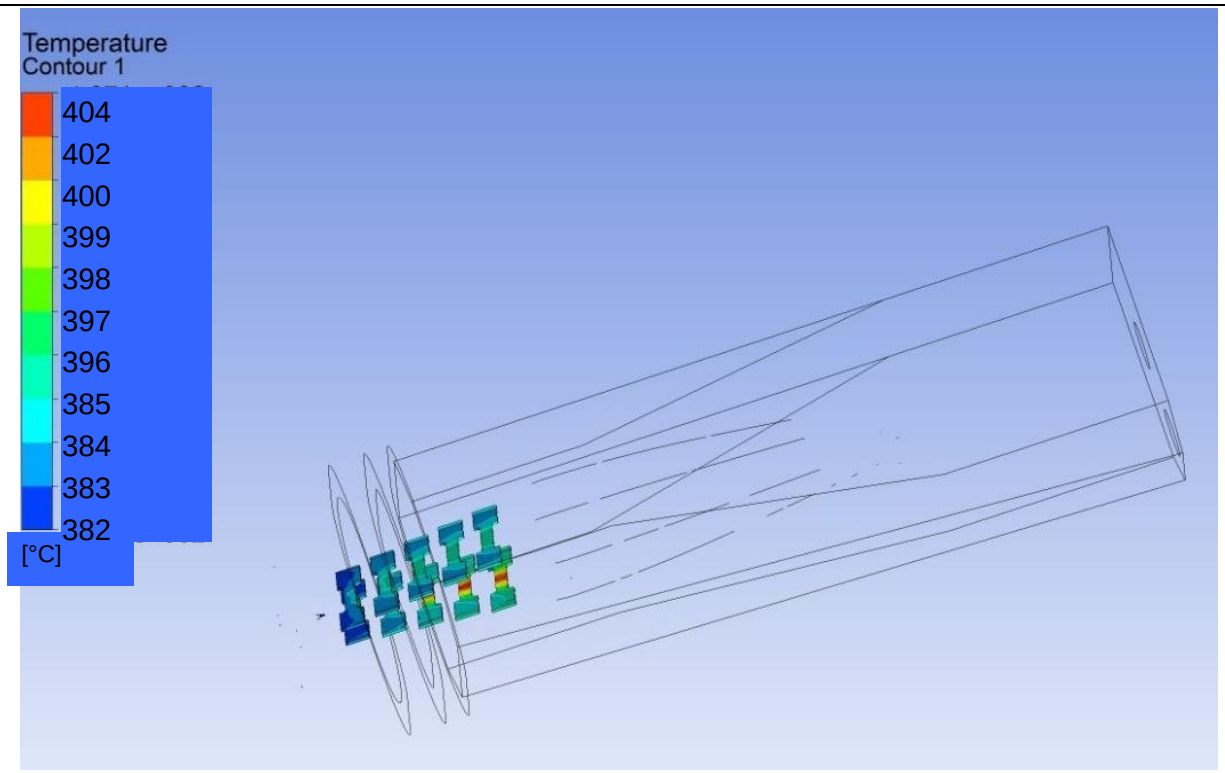


**Figure 21: Temperature contour in the samples at 38 kg/s**

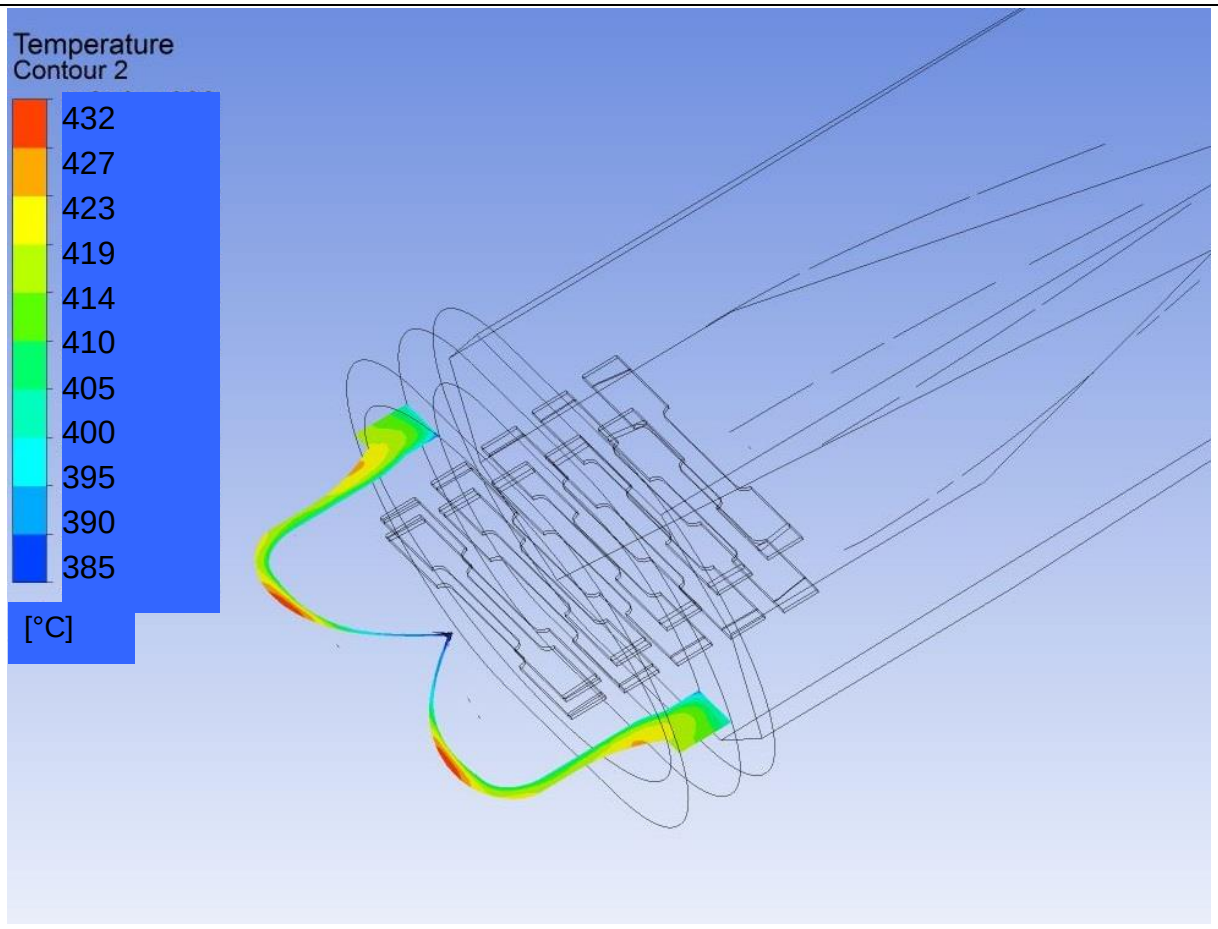


**Figure 22: Temperature contour in the window at 38 kg/s**

Finally, the pressure drop is calculated along the flow path, as shown below.

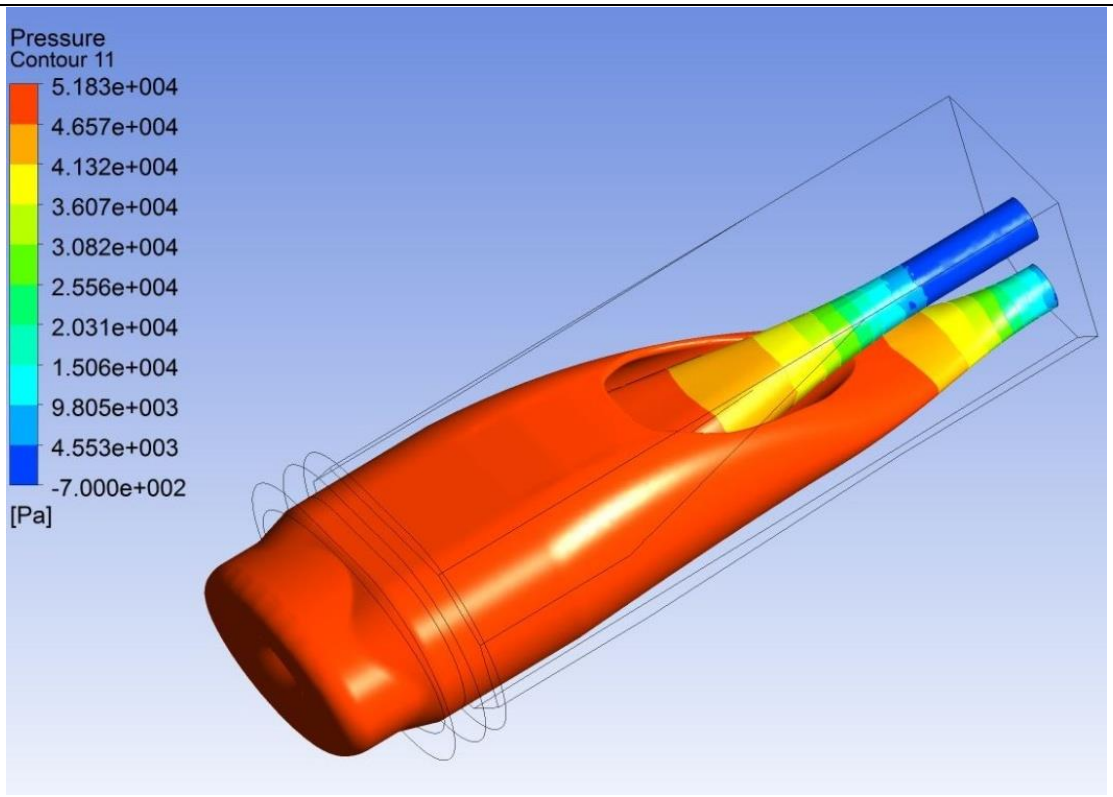


**Figure 23: Pressure profile in fluid domain at 38 kg/s**

The flow of liquid metal is shown in the figure below, from the inlet to the window and around the samples.

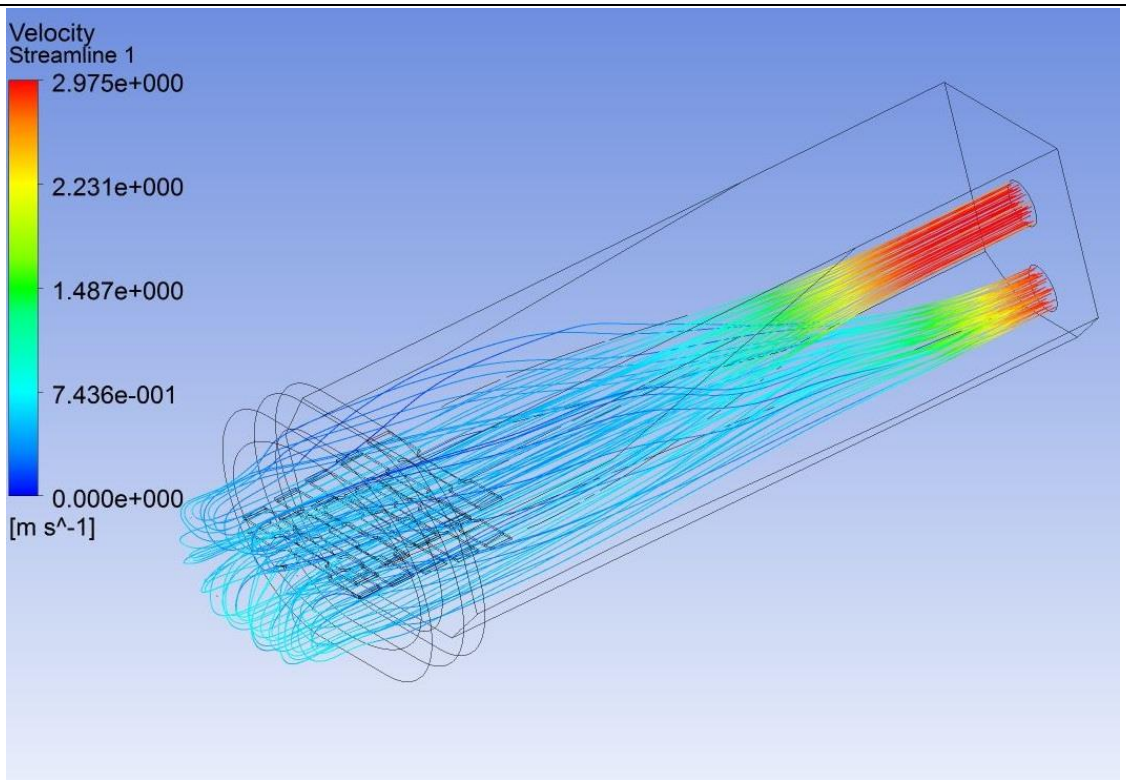


**Figure 24: Velocity streamlines in the fluid at 38 kg/s**

## 3.2 Analysis of the optimised design

In this section the optimised design from chapter 2 is analysed thermally using the baseline assumptions listed in 2.1. The flow rate is varied from a minimum of 4.1 kg/s to a maximum of 38 kg/s in order to vary the sample temperature using the same beam power deposition.

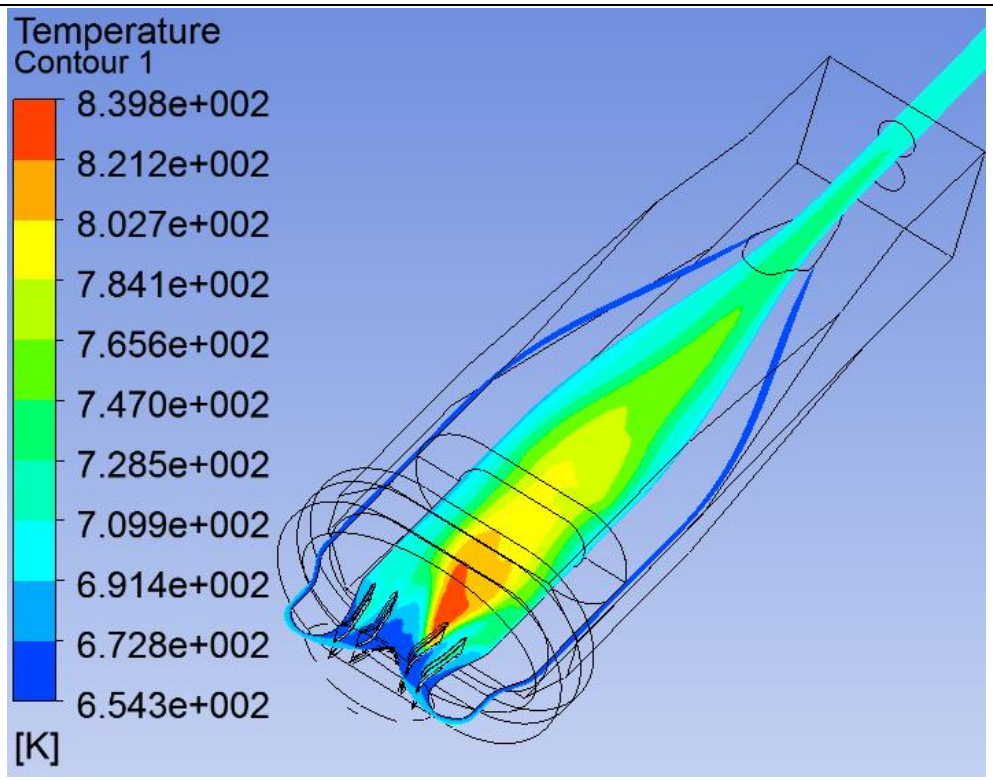


**Figure 25: Temperature contour in central plane in fluid region at 4.1 kg/s**

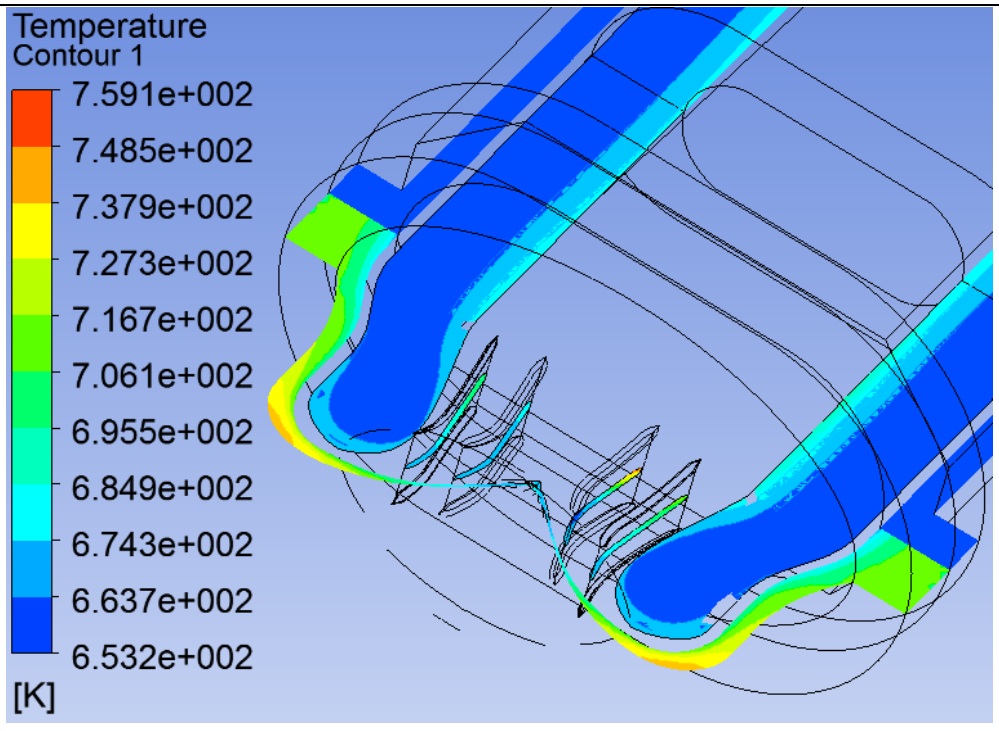


**Figure 26: Temperature contour in central plane in window at 4.1 kg/s**

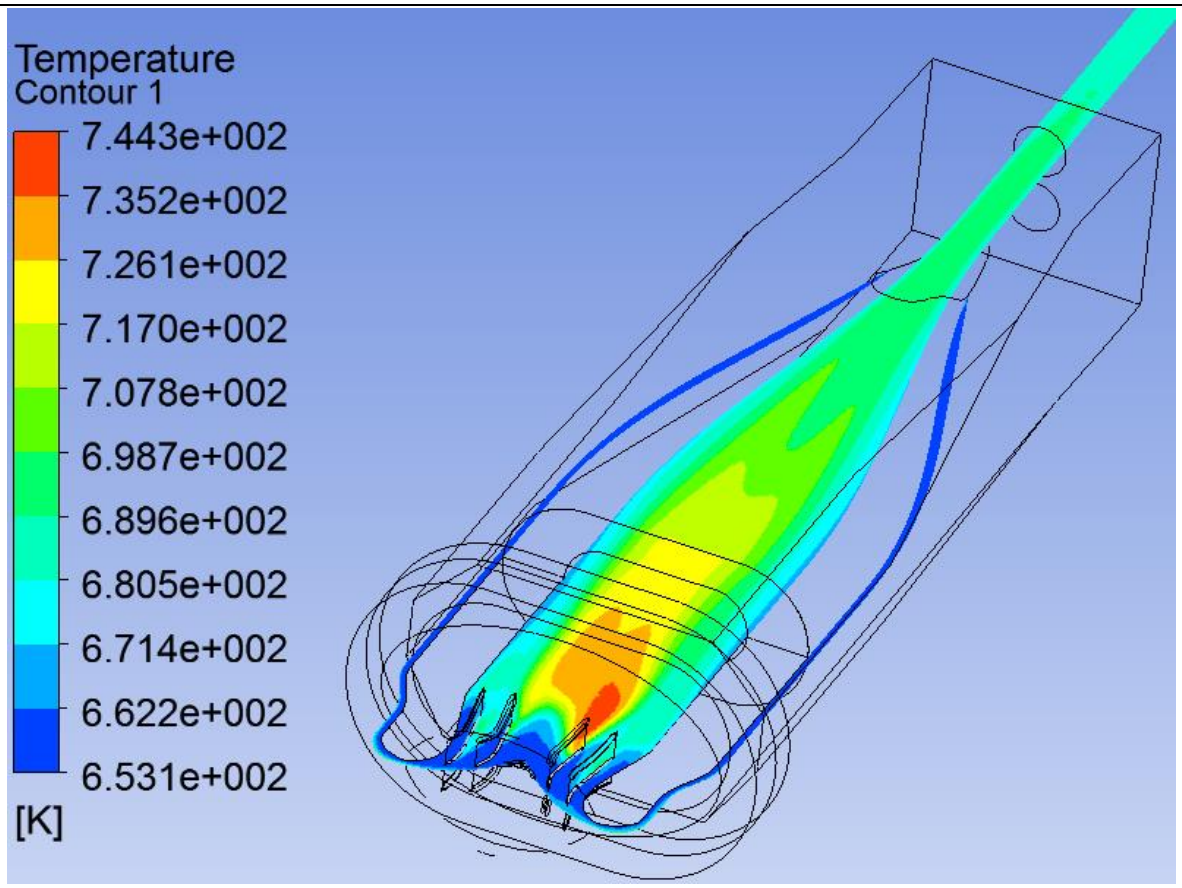


**Figure 27: Temperature contour in central plane in fluid region at 12.3 kg/s**

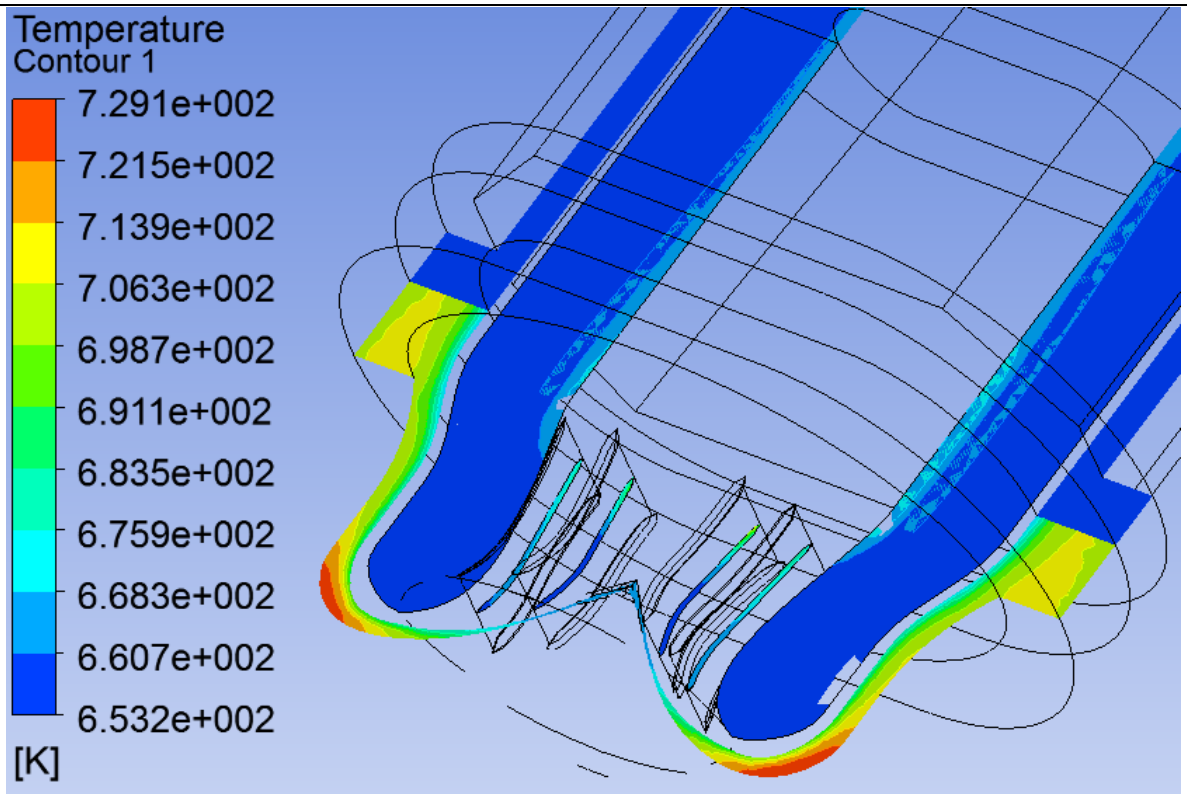


**Figure 28: Temperature contour in central plane in window at 12.3 kg/s**

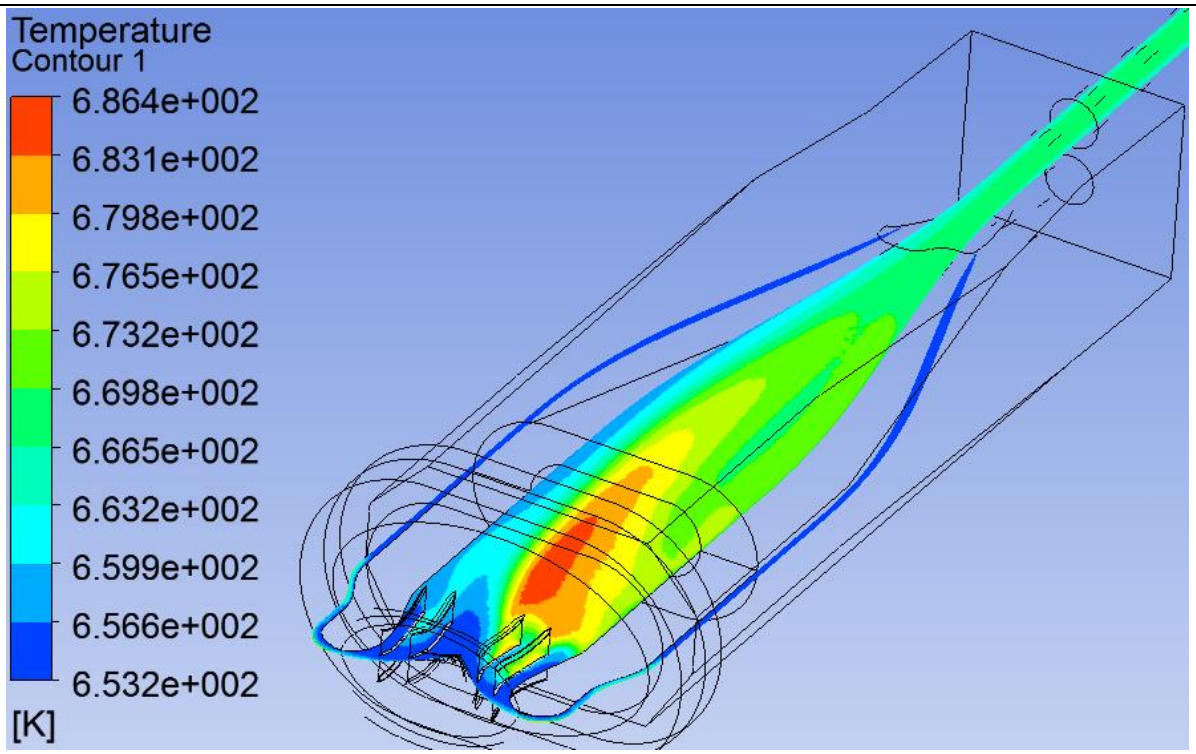


**Figure 29: Temperature contour in central plane in fluid region at 38 kg/s**

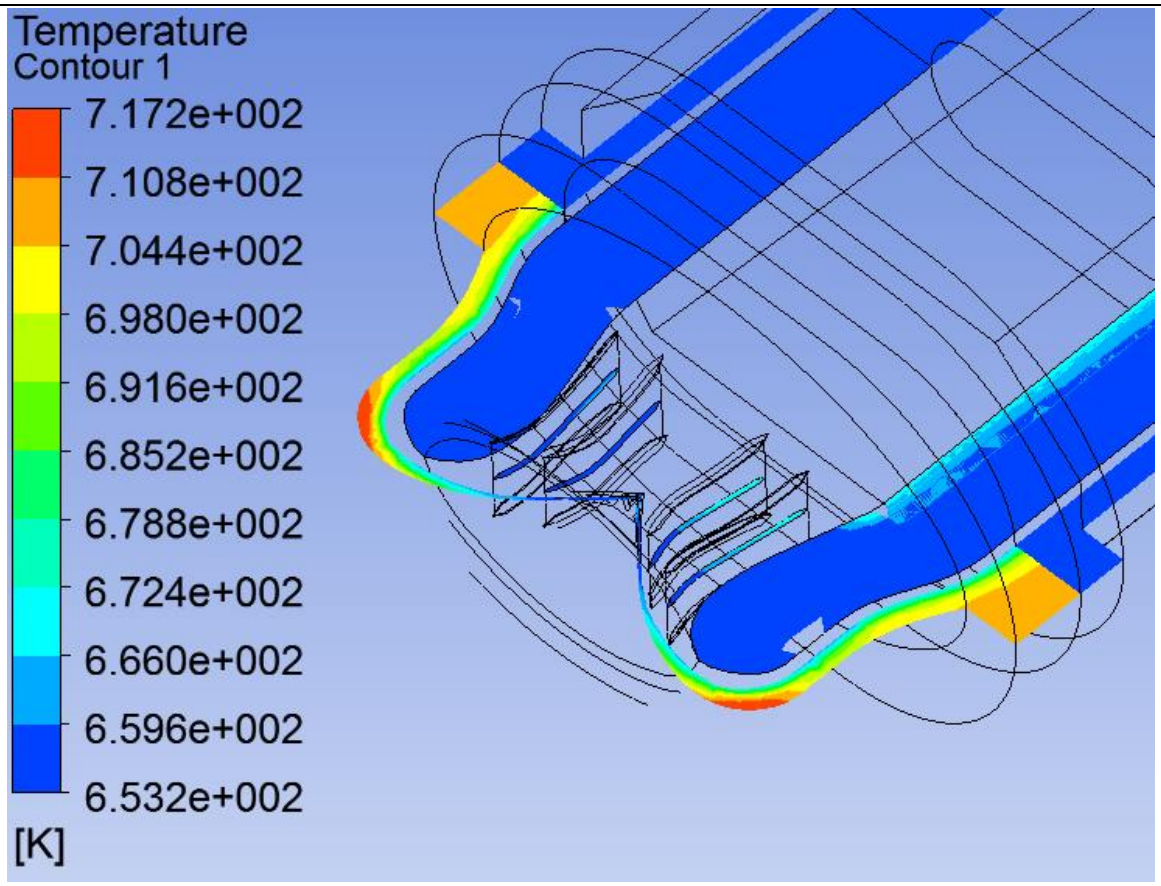


**Figure 30: Temperature contour in central plane in window at 38 kg/s**

As expected, reducing the flow rate in the target increases the temperature of the fluid and therefore the temperature of the samples. Decreasing the mass flow rate from 38 kg/s to 4,1 kg/s makes the temperature around the samples increase from 400 °C to 537°C. This increases also slightly the maximum temperature in the window from 440°C to 467°C.

The effect of increasing the flow rate on the pressure loss through is significant; it increase form 0,05 Bar to 4 bar, remains however tolerable in terms of pumping capacity.

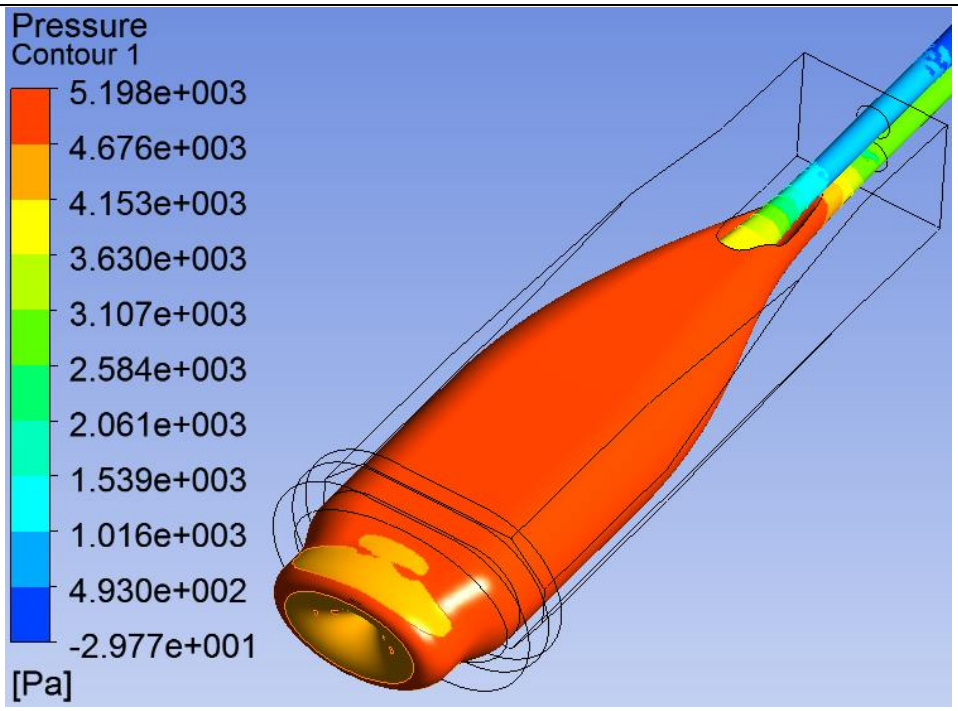


**Figure 31: Pressure in the fluid at 4.1 kg/s**

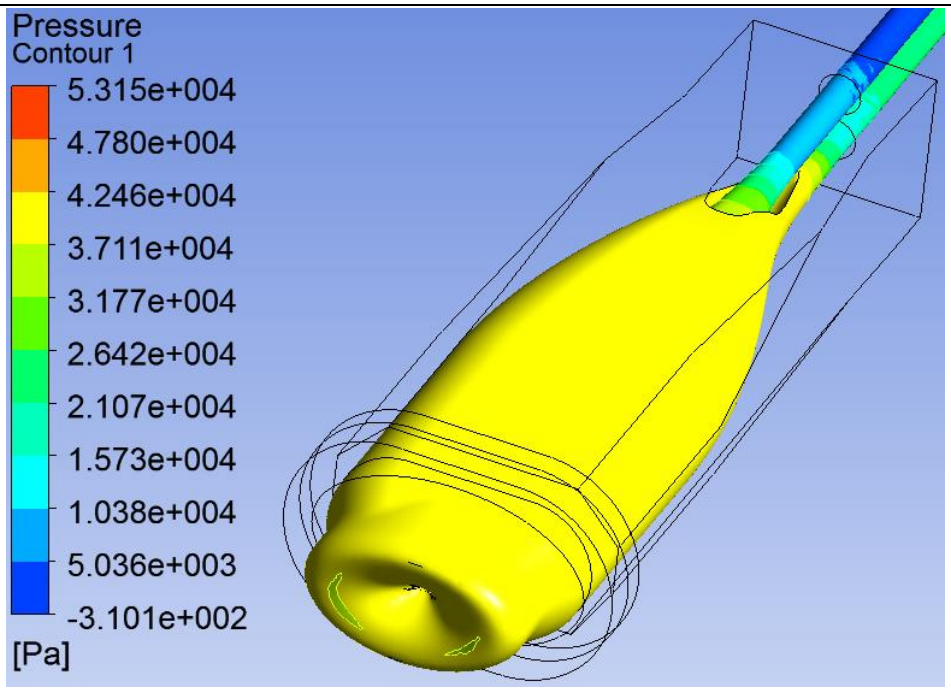


**Figure 32: Pressure in the fluid at 12.3 kg/s**

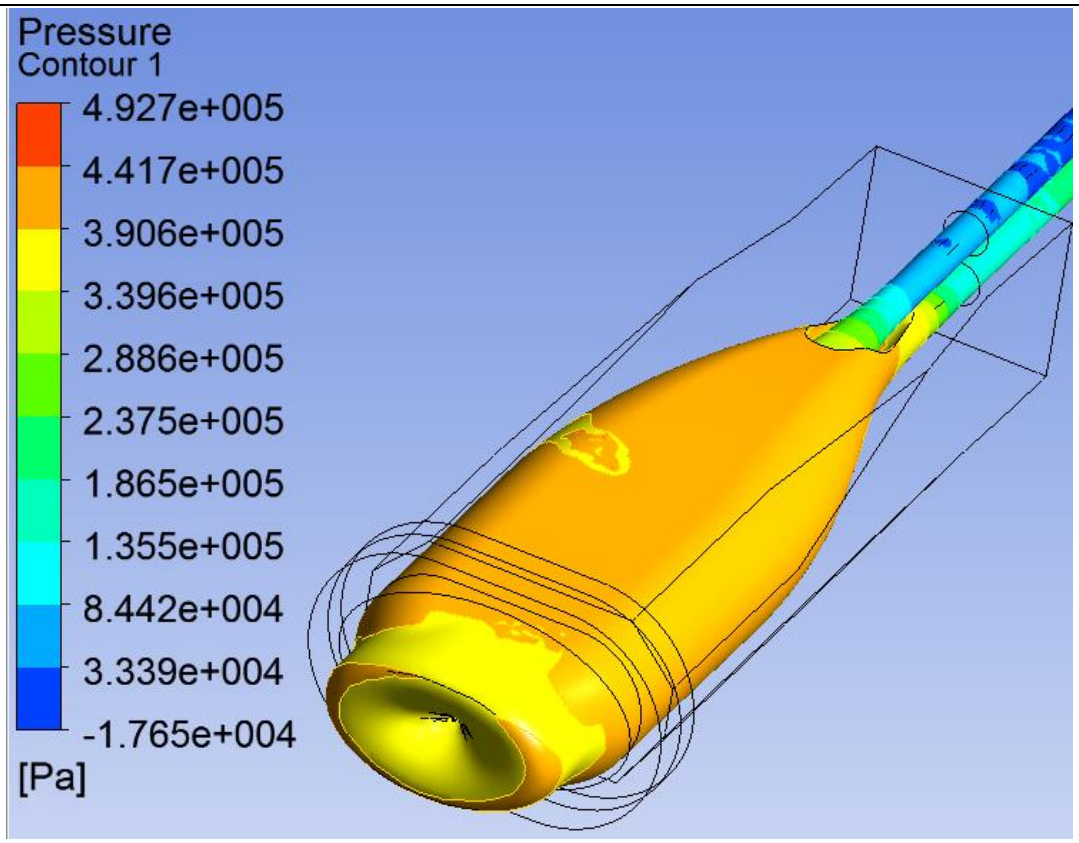


**Figure 33: Pressure in the fluid at 38 kg/s**

In spite of the great change in velocity of the fluid in the target, from 0.25 m/s to 3 m/s, the stability of flow remains unperturbed.

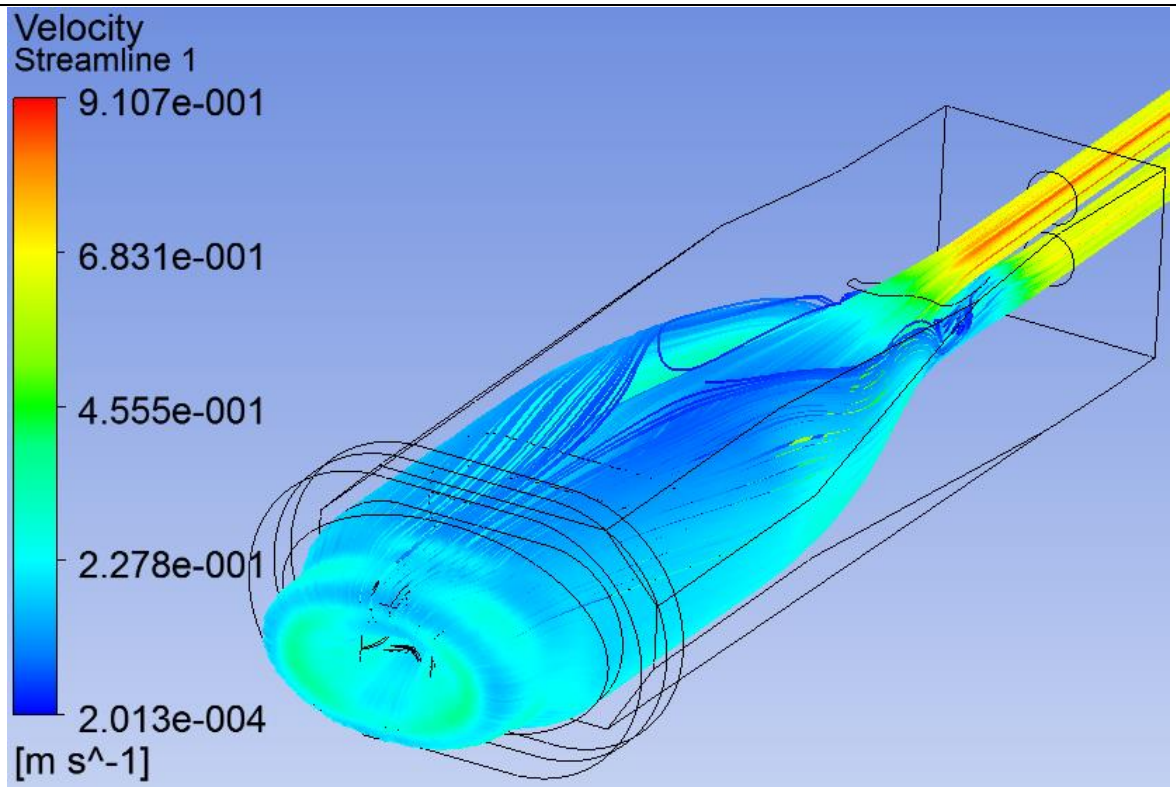


**Figure 34: Velocity in the fluid at 4.1 kg/s**

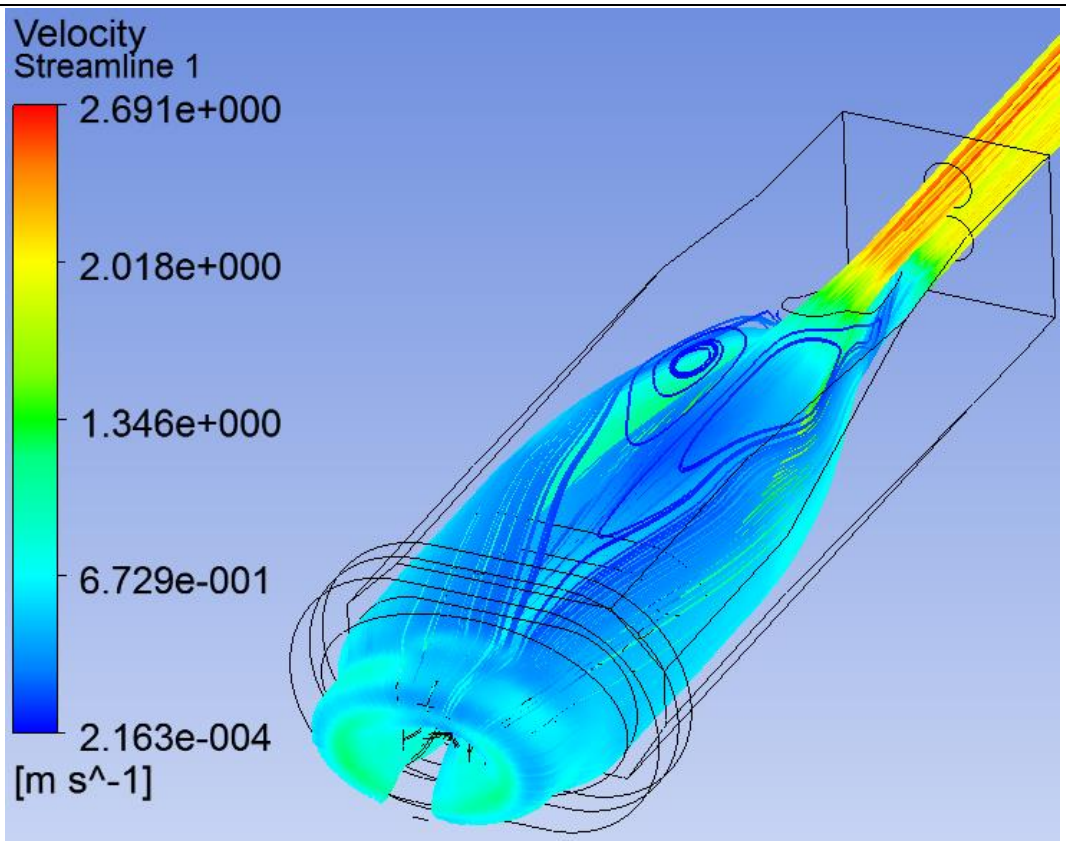


**Figure 35: Velocity in the fluid at 12.3 kg/s**

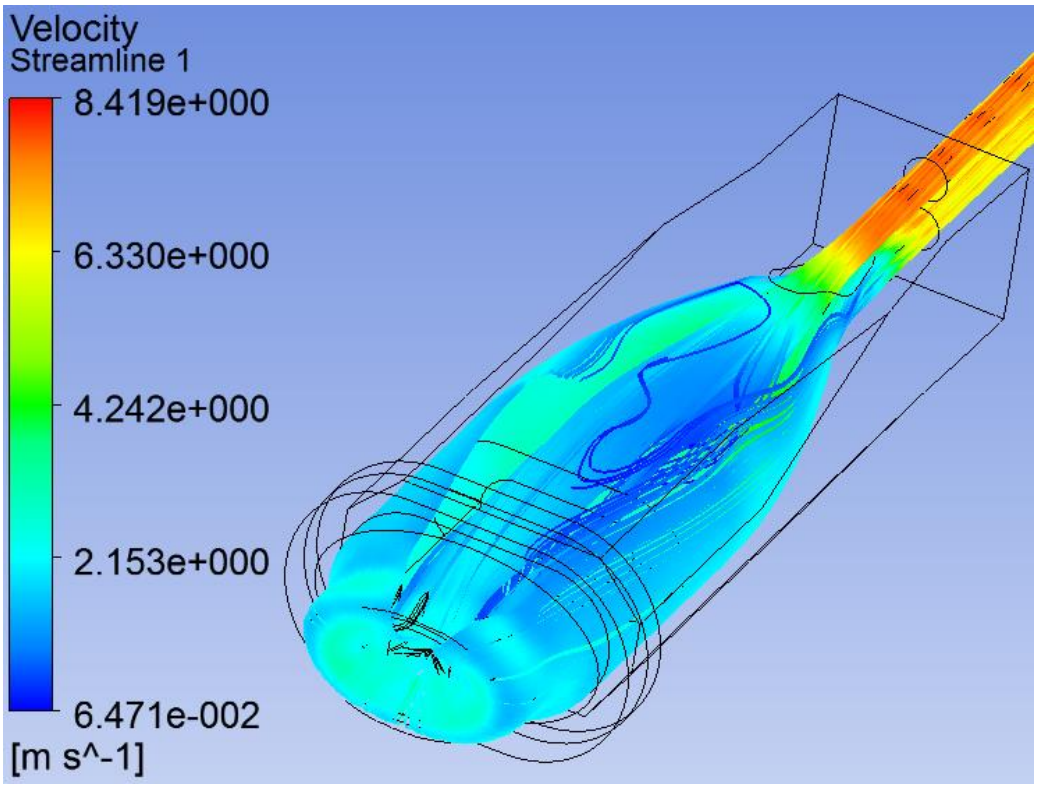


**Figure 36: Velocity in the fluid at 38 kg/s**

In view of these results, changing the flow rate to increase the samples temperature seems a viable option, which has the advantage of not requiring changing the power level in the beam.

# 4 Conclusions

Hydraulic analysis of the target concludes that the essential parameters as laid out in the original preliminary design report (ref.2) are valid and stable conditions will be reached on the window allowing it to be cooled. The use of vanes in reversing the flow back into the guide tube is somewhat novel but due to their attachment method, this is not feared to result in any fatigue failure. Previous testing in the Eurisol program reinforces this belief.

Stress analysis concluded that the thermal loading caused by the beam will not result in strength failure, taking into account the likely weakening of the structure caused by higher irradiation doses. The ability of stainless steel to sustain high DPA has been proven in experiments such as Megapie.